

AD-A164 193

NONLINEAR DYNAMIC RESPONSE OF COMPOSITE ROTOR BLADES

1/1

(U) TEXAS A AND M UNIV COLLEGE STATION DEPT OF
MECHANICAL ENGINEER. J J ENGBLOM ET AL. SEP 84

UNCLASSIFIED

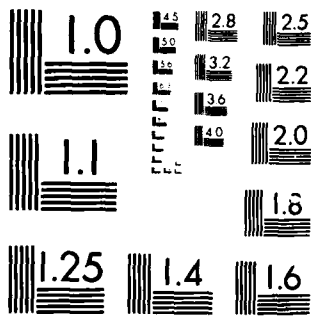
AE-4786-84-9 AFOSR-TR-85-1235

F/G 11/4

NL

END

FORM
144
1-71



MICROCOPY RESOLUTION TEST CHART
NATIONAL BUREAU OF STANDARDS 1963-A

2

AFOSR-TR-



TEXAS A&M UNIVERSITY
College Station, Texas

AD-A164 193

NONLINEAR DYNAMIC RESPONSE
OF
COMPOSITE ROTOR BLADES

Technical Report

Prepared by

Dr. John J. Engblom
and
Dr. Ozden O. Ochoa

of the

Mechanical Engineering Department
Texas A&M University

DISTRIBUTION STATEMENT A
Approved for public release;
Distribution Unlimited

Submitted to the

Air Force Office of Scientific Research
United States Air Force

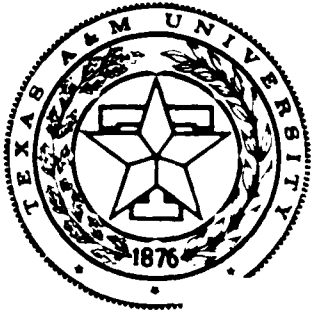
ME 4786-84-9

Contract No. F49620-82-K-0032

September 1984

DTIC
SELECTE
FEB 13 1986
S D

DTIC FILE COPY



TEXAS A&M UNIVERSITY
College Station, Texas

NONLINEAR DYNAMIC RESPONSE
OF
COMPOSITE ROTOR BLADES

Technical Report

Prepared by

Dr. John J. Engblom
and
Dr. Ozden O. Ochoa

of the

Mechanical Engineering Department
Texas A&M University

Submitted to the

Air Force Office of Scientific Research
United States Air Force

ME 4786-84-9

Contract No. F49620-82-K-0032

September 1984

UNCLASSIFIED

SECURITY CLASSIFICATION OF THIS PAGE (When Data Entered)

REPORT DOCUMENTATION PAGE		READ INSTRUCTIONS BEFORE COMPLETING FORM	
1. REPORT NUMBER AFOSR TR-85-1235	2. GOVT ACCESSION NO.	3. RECIPIENT'S CATALOG NUMBER	
4. TITLE (and Subtitle) Nonlinear Dynamic Response of Composite Rotor Blades		5. TYPE OF REPORT & PERIOD COVERED Annual Report 1 Sept 1983 - 31 Aug 1984	
7. AUTHOR(s) John J. Engblom, Ozden O. Ochoa		6. PERFORMING ORG. REPORT NUMBER ME 4786-83-10	
9. PERFORMING ORGANIZATION NAME AND ADDRESS Texas A&M University Mechanical Engineering Department College Station, TX 77843		8. CONTRACT OR GRANT NUMBER(s) F49620-82-K-0032	
11. CONTROLLING OFFICE NAME AND ADDRESS Air Force Office of Scientific Research / NA Building 410 Bolling AFB, DC 20332		10. PROGRAM ELEMENT, PROJECT, TASK AREA & WORK UNIT NUMBERS G1102F 2302/B1	
14. MONITORING AGENCY NAME & ADDRESS (if different from Controlling Office)		12. REPORT DATE September 1984	
		13. NUMBER OF PAGES 70 plus Appendices	
		15. SECURITY CLASS. (of this report) Unclassified	
		15a. DECLASSIFICATION DOWNGRADING SCHEDULE	
16. DISTRIBUTION STATEMENT (of this Report) Approved for Public Release, Distribution Unlimited			
17. DISTRIBUTION STATEMENT (of the abstract entered in Block 20, if different from Report)			
18. SUPPLEMENTARY NOTES			
19. KEY WORDS (Continue on reverse side if necessary and identify by block number) Composite Materials; Interlaminar Shear and Normal Stresses; Nonlinear Dynamic Response; Assumed Displacement and Hybrid Models. Damage Mechanisms Finite Elements Large Displacement Formulation			
20. ABSTRACT (Continue on reverse side if necessary and identify by block number) Summarized are research activities related to Nonlinear Dynamic Response of Composite Rotor Blades. Fundamental to the analysis is the development of a continuum formulation that can accurately account for the effects of interlaminar shear and interlaminar normal stress variation thru-the-thickness of a laminate. Technical highlights of the research efforts to date are presented for each of the proposed tasks; namely, Nonlinear Displacement Formulation for Composite Media, Incorporate Damage Mechanisms into Dynamic Response Formulation and Correlation of Formulated Response Model with Experimental data.			

TABLE OF CONTENTS

	Page
I. Overview and Summary	1
II. Summary by Task	3
II.1. Task I: Nonlinear Displacement Formulation for Composite Media	3
II.1.1 Continuum Formulation	3
II.1.2 Large-Displacement Formulation	6
II.1.3 Computer Implementation	9
II.1.4 Analytical Verification	13
II.2. Task II: Incorporate Damage Mechanisms into Dynamic Response Formulation	20
II.3. Task III: Correlation of Formulated Response Model with Experimental Data	22
III. References	23
IV. Tables and Figures	31
V. Related Activities	69
VI. Appendices	

AIR FORCE OFFICE OF SCIENTIFIC RESEARCH (AFOSR)

NOTICE OF TRANSMISSION

This report is being transmitted to you for your information.

and

to

to

Chief, Research and Development Division



Accession For	
NTIS CRA&I	<input checked="" type="checkbox"/>
DTIC TAB	<input type="checkbox"/>
Unannounced	<input type="checkbox"/>
Justification	
By	
Distribution:	
Availability Codes	
Dist	Avail and/or Special
A-1	

I. OVERVIEW AND SUMMARY

Fundamental to this work is the development of a continuum formulation that can accurately account for the effects of interlaminar shear and interlaminar normal stress variation thru-the-thickness of a laminate. Furthermore, emphasis is particularly on tapered-twisted airfoil geometries which can be analytically represented as an assemblage of thin to moderately thick finite elements. To achieve solution efficiencies, the elements developed in this work are of the triangular/quadrilateral plate type as opposed to solid type elements.

On the basis of these requirements and considering viable alternatives, three suitable continuum formulations have been developed and are herein denoted as the (i) Higher Order Displacement, (ii) Modified-Kirchhoff and (iii) Hybrid Stress formulations, respectively. The former two formulations have been incorporated in a computer code and the various elements have been tested on the basis of correlations with known analytical, numerical, and experimental solutions. Numerous tests have been performed for linear static and linear dynamic cases. It is noted that the code has some unique features, e.g., it can assemble elements having an unequal number of degrees of freedom at its nodes, it treats arbitrary ply orientations and it performs integration on a layer-by-layer basis through the laminate. Herein a layer refers to either a lamina or to a sub-set of laminae having equal ply orientations. The latter feature is essential in developing a fully nonlinear capability.

Significant efforts have also been devoted to developing a

suitable large displacement formulation. Due to the requirement that interlaminar stresses be accurately represented, a total Lagrangian formulation is utilized and is based upon the complete Green's strain tensor. A geometric and large-displacement stiffness formulation has been implemented in the computer code based upon a form of the nonlinear strain-nodal displacement relationships suitable for each of the elements under development.

An extensive literature survey has been performed to identify analytically tractable methods of treating damage accumulation in composites. Since emphasis in this work is on the development of incremental response solutions, the computational approach must have the capability to (i) predict and differentiate between relevant failure modes, (ii) modify constitutive equations appropriately and (iii) perform equilibrium iterations to assure stress redistribution based upon the extent of damage. Use of "piecewise smooth" failure criteria in conjunction with "damage state" variables provide a good basis for incrementally tracking damage. This approach has been incorporated in the computer code. Note that integration for an element is performed on a layer-by-layer basis which allows for damage effects to be characterized at the layer level.

Experimental data of the type required to substantiate damage predictions has been assembled to the extent possible. Analysis/test correlations have been performed for selected laminates. It is noted that useful experimental data is quite limited.

Technical progress in this program has been substantially on schedule. It is believed that the originally proposed three year program can be completed within the given time frame.

II. SUMMARY BY TASK

This section presents technical highlights of the research efforts to date for each of the three tasks. Details of the analytical formulation are presented in the Appendices.

II.1. TASK I: Nonlinear Displacement Formulation for Composite Media

II.1.1 Continuum Formulation

Two variational principles, the principle of Minimum Potential Energy and the Principle of Modified Complementary Energy, are used to develop two distinctly different finite element models, the assumed displacement model and the hybrid stress model respectively. These models incorporate the effects of transverse shear and normal deformations whose contributions are recognized as essential for accurate laminate analysis [1-10].

Within each formulation, element stiffness and force matrices are determined for each element, these matrices are then assembled to represent the final system of equations and a solution procedure for the unknown nodal displacements is provided. Coordinate transformations to describe ply orientations of a composite media are taken into account. The in-plane stresses are calculated from constitutive relations of orthotropic continuum whereas transverse shear and normal stresses are calculated from equilibrium considerations. At present, emphasis is placed on the displacement

based models and these have been tested for linear static and dynamic analysis. The test problems and the results are presented in Section II.1.4. The finite element models are herein briefly discussed.

i. Assumed Displacement Model

A. Higher Order Displacement Formulation

The thru-the-thickness effects can be incorporated into an analysis by choosing a displacement field that eliminates two major shortcomings of the classical plate theory; namely normals remain normal and in-plane displacements are linear thru the thickness. These shortcomings are eliminated by prescribing independently the reference surface displacements and rotations of the normal and including higher order terms for in-plane displacements. This is accomplished by the following variation

$$\begin{aligned}u(x,y,z) &= u_0(x,y) + z \cdot \psi_x(x,y) + z^2 \phi_x(x,y) \\v(x,y,z) &= v_0(x,y) + z \cdot \psi_y(x,y) + z^2 \phi_y(x,y) \\w(x,y,z) &= w_0(x,y)\end{aligned}$$

The neutral surface displacements are represented by u_0 , v_0 and w_0 , the rotation about y-axis is denoted by ψ_x and the rotation about the x-axis is ψ_y . The coefficients of z^2 , i.e., ϕ_x and ϕ_y , are contributions from transverse deformations [5,6].

The elements developed are designated as the quadrilateral higher order displacement (QHD) models. QHD40 is an eight-noded element with seven degrees of freedom (three midsurface displacements, two

rotations and two higher order terms for in-plane displacements) per corner node and three degrees of freedom (transverse midsurface displacement and two rotations) per mid-side node. Element QHD28 is a simplified version of QHD40 where the mid-side nodes are eliminated. It should be noted that when the two higher order terms for in-plane displacements at each corner node are omitted, QHD28 reduces to the widely used four-noded bilinear plate element (QHD20).

The transverse shear and normal stresses of QHD40 display a cubic variation thru-the-thickness. The displacement field, nodal degrees of freedom and the resulting stress fields are stated in Appendix IA.

B. Modified-Kirchhoff Formulation

The Kirchhoff-Love assumption for normals to the reference surface is relaxed by incorporating shear rotations as additional degrees of freedom in the formulation [10]. Thus the assumed displacement field allows the transverse shear deformations but neglects the transverse normal deformations. The rotations γ_x and γ_y are incorporated in the displacement variation as follows

$$w(x,y) = w_0(x,y)$$

$$u(x,y,z) = u_0(x,y) - z\left(\frac{w}{x} + \gamma_x\right)$$

$$v(x,y,z) = v_0(x,y) - z\left(\frac{w}{y} + \gamma_y\right)$$

The transverse displacement $w(x,y)$ is chosen such that it will guarantee plausible stress fields which will characterize the transverse effects accurately.

This approach is implemented in the formulation of an eight-node quadrilateral element with 32 degrees of freedom- QD32, a six-node triangular element with 27 d.o.f.- TD27 and a seven-node triangular element with 27 d.o.f.- TD27M. The stress fields obtained for these elements represents a quadratic thru the thickness variation for the transverse shear stresses and a cubic variation for the transverse normal stress. The respective displacement fields, nodal degrees of freedom and stress fields are given in Appendix IB.

ii. Hybrid Stress Model

In this formulation a stress distribution within the interior of the element is expressed in terms of finite parameters such that equilibrium is satisfied, also an assumed displacement distribution is used on the boundary of the element expressed in terms of generalized nodal displacements such that the interelement compatibility is retained [4].

The element developed, QHS32, is a four-node quadrilateral with 32 degrees of freedom. In addition to an assumed displacement field it has a 26-parameter stress field which provides cubic variation for transverse shear stresses and a quartic variation for transverse normal stress through the thickness of the laminate. The stress field along with the assumed displacement variation is stated in Appendix II

II.1.2. Large Displacement Formulation

Inclusion of geometrically nonlinear effects in the formulation must be based upon both the geometry to be analyzed and upon the type of stress prediction capabilities desired. The classical approach to thin plate analysis has been to use the Kirchhoff-Love assumptions in

conjunction with the nonlinear von Karman relations [11,12]. As previously indicated, the Kirchhoff-Love assumptions are relaxed in this work to allow for a more accurate definition of interlaminar-shear and interlaminar-normal stress variations. These stresses can vary substantially through-the-thickness for the geometries of interest, i.e., thin to moderately thick plate type structures. Furthermore, the requirement that these stresses be accurately determined means that the nonlinear portion of the strain-displacement relationship must contain all significant coordinate displacements. The complete Green's strain tensor is utilized in this work, therefore, to account for all significant contributions to the interlaminar stress field. With respect to fixed Cartesian coordinates, x , y , and z , the strain tensor has the form

$$\epsilon_x = \frac{\partial u}{\partial x} + \frac{1}{2} \left[\left(\frac{\partial u}{\partial x} \right)^2 + \left(\frac{\partial v}{\partial x} \right)^2 + \left(\frac{\partial w}{\partial x} \right)^2 \right]$$

$$\epsilon_{xy} = \frac{\partial u}{\partial y} + \frac{\partial v}{\partial x} + \left[\frac{\partial u}{\partial x} \frac{\partial u}{\partial y} + \frac{\partial v}{\partial x} \frac{\partial v}{\partial y} + \frac{\partial w}{\partial x} \frac{\partial w}{\partial y} \right]$$

where u , v and w represent displacements in the x, y, z coordinate directions, respectively. Note that the other strain components are obtained by a suitable permutation. In small-displacement analysis, the quadratic terms are neglected to give simply the linear strain approximation.

Based on the Green's strain tensor, the strain to nodal point displacement relationship can be specified for elements under

development. It takes the form

$$\{\epsilon\} = [B]\{\Delta\}$$

where $\{\epsilon\}$ is the vector of strain components, $\{\Delta\}$ the vector of nodal point displacements and $[B]$ a function of derivatives of the element shape functions. The quadratic terms in the strain tensor result in $[B]$ being a function of displacement state and, therefore, an incremental equilibrium formulation is required. The incremental strain-nodal displacement relationship takes the form

$$\{\delta\epsilon\} = ([B_0] + [B_L])\{\delta\Delta\}$$

where $\{\delta\epsilon\}$ and $\{\delta\Delta\}$ represent incremental strains and nodal displacements, respectively, $[B_0]$ and $[B_L]$ are the small and large displacement contributions to the incremental strains. Based on the incremental equilibrium equations, the displacement formulation gives the force-displacement relationships

$$[K_0] = \int_V [B_0]^T [D] [B_0] dV$$

$$[K_L] = \int_V ([B_0]^T [D] [B_L] + [B_L]^T [D] [B_L] + [B_L]^T [D] [B_0]) dV$$

where $[D]$ is an elasticity matrix obtained simply from the constitutive equations and integration is over the volume V of the element. $[K]$ is denoted the small-displacement stiffness matrix and $[K_L]$ is denoted the large-displacement stiffness matrix. Since response is also a function of stress state, the geometrical stiffness matrix $[K_G]$ is required and is obtained from

$$[K_G] = \int_V [B_L]^T [D] [B_L] dV$$

where $\{\sigma\}$ is the vector of stress components. Note that the hybrid stress formulation similarly gives force-displacement forms involving the stress and displacement state.

Inertial effects are analytically treated as a mass matrix $[M]$ which is a function of density and the element shape functions (see Appendix III). These matrix forms are required in formulating static/dynamic response solutions and the incremental equilibrium have the general form

$$[M](\delta\ddot{u}) + ([K_0] + [K_L] + [K_G])\{\delta u\} = \{\delta F\}$$

where the mass and stiffness matrices represent an assembly of the elemental matrices previously discussed, $\{\delta u\}$ and $\{\delta\ddot{u}\}$ represent the incremental displacements and accelerations for the mathematical model and $\{F\}$ represents the vector of incrementally applied forces.

In developing a geometrically nonlinear formulation, the effort is largely in defining the incremental strain-nodal displacement relationship. Having developed this relationship for a particular element, stiffness matrices are readily developed as the preceding equations indicate. These relationships are presented in Appendix IV. The form of these equations is the same for all elements.

II.1.3. Computer Implementation

A computer code has been developed for the purpose of implementing the various continuum formulations. At present, the code

performs the following functions:

- element stiffness matrix (linear, nonlinear, geometric) generation
- element mass matrix generation
- assembly of equilibrium equations
- decomposition and solution of equilibrium equations
- equilibrium iteration for incremental solutions
- fundamental frequency and mode shape calculation

A characteristic of the elements under development is that node points can have different numbers of degrees of freedom, i.e., typically mid-side nodes have fewer degrees of freedom than corner nodes. The code has been fashioned to handle this condition. All of the integration is performed on a layer-by-layer basis thru the thickness of the laminate. This approach is fundamental to developing the capability to allow for inelastic material behavior and, ultimately, to the inclusion of damage mechanisms in the formulation.

Since solution of the equilibrium equations is a vital component in the overall solution strategy, it is appropriate to discuss the numerical methodology used in solving these equations. The intent is to obtain a higher ordered variation of the transverse shear and normal stresses (σ_{xz} , σ_{yz} , and σ_{zz}) than can be obtained via the constitutive equations. The solution procedure can be thought of as described below. Assume that the in-plane stresses (σ_{xx} , σ_{yy} , σ_{xy}) within each layer of a particular element have been determined at selected locations, i.e., through solution of the constitutive equations. In the code as presently written, these locations are specified as the element centroid and element nodal points. The

equilibrium equations (in the absence of body forces) have the indicial form

$$\sigma_{ij,j} = 0$$

from which it follows that the thru-the-thickness shear stress variation can be written in numerical form for the i^{th} layer as

$$\Delta\sigma_{xz_i} = -(\sigma_{xx,x} + \sigma_{xy,y})_i \Delta Z_i$$

and

$$\Delta\sigma_{yz_i} = -(\sigma_{xy,x} + \sigma_{yy,y})_i \Delta Z_i$$

Here, the left-hand-side represents the change in stress from the lower to the upper surface of the i^{th} layer and ΔZ_i is the thickness of the i^{th} layer at a particular location. The derivatives with respect to x and y in the expressions above are readily computed; this is because in-plane stresses within a layer are related to element displacements through derivatives of element shape functions in conjunction with a material definition.

For an n layered laminate, n equations can be written in terms of both the unknown shear stresses at layer interfaces and the shear stresses at the laminate surfaces. Assuming the laminate has shear-free surfaces, the equations above give n equations in $n-1$ unknowns, so that, the equation set is over-determined. The equations have the matrix form below

$$\begin{bmatrix} 1 & & & & \\ -1 & 1 & & & \\ & -1 & 1 & & \\ & & & \ddots & \\ & & & & 1 \\ & & & & -1 \end{bmatrix} \begin{Bmatrix} \sigma_{xz_2} \\ \vdots \\ \sigma_{xz_n} \end{Bmatrix} = \begin{Bmatrix} I_{xz_1} \\ \vdots \\ I_{xz_n} \end{Bmatrix}$$

$n \times (n-1) \quad (n-1) \times 1 \quad (n \times 1)$

where $I_{xzi} = -(\sigma_{xx,x} + \sigma_{xy,y})_i \Delta Z_i$ and σ_{xzj} represents the shear stress acting at the interface of the $(j-1)^{\text{th}}$ and j^{th} layer. A similar equation set is obtained by replacing σ_{xzj} with σ_{yzj} and I_{xzi} with I_{yzi} . These equations are solved by utilizing a least-squares orthonormalization procedure [13]. Due to the simplicity of the terms in the coefficient matrix, a concise closed-form solution is obtained. Having determined the transverse shear stresses, the transverse normal stress variation is determined through the numerical form of the third equilibrium equation for the i^{th} layer

$$\Delta \sigma_{zzj} = -(\sigma_{xz,x} + \sigma_{yz,y})_j \Delta Z_j$$

As before, the left-hand-side represents the change in stress through the i^{th} layer. Appropriate polynomial functions are utilized to describe the σ_{xz} and σ_{yz} in-plane variation. These functions are differentiated to obtain the right-hand-side of the equations above. Again the equation set is overdetermined because the normal tractions are known at the laminate surfaces. Solving for σ_{zz} proceeds, therefore, in identically the same manner as discussed in calculating σ_{xz} and σ_{yz} . Parenthetically, inclusion of body forces at a later date can be accomplished with little difficulty.

It should be emphasized that, the successful application of Higher Order Displacement type elements, i.e., for particularly thin

geometries, is to utilize reduced numerical integration where as this is not necessary for the Modified Kirchhoff formulation. This approximation technique brings along the choice of implementing it overall or selectively to the strain energy components. For the QHD formulation, only the transverse shear components are integrated with reduced order [14-16]. An undesirable aspect of this approach is that the reduced integration order may affect the physical behavior of the element by introducing spurious zero energy modes. It is desirable to have only rigid body modes since there does not yet seem to be a generally accepted method of controlling the additional modes.

II.1.4. Analytical Verification

As noted, elements formulated on the basis of independent transverse displacements and rotations, require reduced quadrature for good performance. For QHD40, 3x3 Gaussian quadrature along with the 2x2 quadrature for the transverse shear components is employed. QHD28 and QHD20 formulations are similarly integrated with 2x2 and 1x1 Gaussian quadratures. Manipulation of quadrature rules may produce spurious zero energy modes in addition to the required rigid body modes, thus detracting from overall element performance. [16,17]. A spectral (eigenvalue) test has been conducted with and without full quadrature to observe the zero energy modes of the QHD elements. The quadrature order, the number of zero eigenvalues and the corresponding number of spurious zero energy modes for the QHD40, QHD28, and QHD20 elements are listed in Table 1. The spurious mode shapes associated with the QHD28 element are illustrated in Figure 1. Since the QHD40

formulation does not exhibit spurious modes, it can be utilized in modelling complex geometries without concern for controlling such behavior.

It is also noteworthy to observe the effect of reduced integration on the representation of the generalized forces. In order to illustrate the effect, the forces associated with the transverse displacement of a corner node are sketched in Fig. 2 for QHD28 with and without reduced integration respectively.

In the examples that follow, performance of the QHD formulation is demonstrated by comparing results to those obtained by classical plate theory (CPT), by elasticity and by other finite element formulations for linear static and linear dynamic analyses. Some results are also presented for the QD formulation. The orthotropic material properties used throughout are tabulated in Table 2. Geometries studied include cylindrical bending of a plate as well as bending of simply supported square and rectangular plates. Various ply layups are considered and loading is that of a sinusoidally and uniformly distributed pressure. Cylindrical bending is modelled as a strip of twenty elements. For the simply supported plates, symmetry considerations allow that only a quadrant of the plate need be modelled. Fineness of the mesh is varied to demonstrate solution convergence. Additionally, distorted meshes are considered to demonstrate modelling considerations. For the examples involving symmetric layups, the quadratic terms of QHD40 are restrained; so that, 32 degree of freedom elements are utilized to obtain these solutions. This is allowable in these particular cases because the quadratic terms do not significantly affect the results. This is not

true in the first example considered.

Static Response Calculations

Cylindrical Bending- Bidirectional (0 /90) Sine Load, Material II

Fibers run parallel to the plane of curvature in the lower layer and are rotated 90° in the upper layer of the plate. Layers are of equal thickness which is true in the subsequent example problems as well. The elasticity solution obtained by Pagano [9] gives a nearly quadratic z variation in \bar{u} , where \bar{u} is the normalized in-plane displacement of the laminate. In this instance, inclusion of the z^2 terms in the finite element modelling should affect the results. This is demonstrated in Figures 3 to 5. Results demonstrate differences obtained with and without *quadratic* terms. The difference is greatest for the lower aspect ratios, e.g., for $S = 4$ a difference of 12% is obtained. In Figure 4, the calculated normalized in-plane stress variation is presented for an aspect ratio of 4. Note that maximum stresses differ by some 36% when computed with and without the z^2 terms, respectively. The effect of including quadratic terms in the finite element solution is, therefore, much more pronounced when stresses as opposed to displacements are considered. Figure 5 demonstrates this effect on stress computation as a function of aspect ratio. Note that calculated quantities are normalized in this example and in those that follow as in the cited references.

Cylindrical Bending-Symmetric (0 /90 /0)Sine Load, Material II

For this geometry, fibers are parallel to the plane of curvature

in the outer layers and rotated 90° in the middle layer. Calculated stresses are compared to the elasticity solution of Pagano [9]. Figures 6 and 7 present the normalized transverse shear stress variation at the simply supported boundary. Figures 8 and 9 present the normalized in-plane stress variation at the center of the bent surface.

Simply Supported Square Plate- (0 /90 /0) Sine Load, Material II

Fibers in the outer layers of the laminate run parallel to the x axis while those in the middle layer run parallel to the y axis, where the origin of coordinates is located at a corner of the plate and in the mid-plane (see Figure 10). This coordinate system is consistent with examples that follow as well. Consider the plate as having planar dimensions $a \times a$ and total thickness h . Solutions have been generated for aspect ratios $S = 4$ to 100, where $S = a/h$. Transverse shear stress variation σ_{xz} at (x,y) coordinates $(0,a/2)$ and in-plane shear stress variation σ_{xy} at coordinates $(0,0)$ are presented in Figures 10 and 11 for an aspect ratio of 4. Note that the comparison is between the present finite element results and those obtained via elasticity [18] and CPT. Calculated short-transverse normal stress variation σ_{zz} is presented in Figures 12 and 13. These stresses are normalized as $\bar{\sigma}_{zz} = \sigma_{zz}/100$ at the center of the plate and as $\sigma_{zz} = 10\bar{\sigma}_{zz}$ at the edge of the plate. Results are compared to those obtained by elasticity over a range of aspect ratios in Table 3. Similar results are given in Table 3.1 for the QD formulation. Convergence characteristics are demonstrated by presenting results obtained using 2×2 , 3×3 , and 6×6 meshes. The finer mesh gives better agreement, but

the coarser mesh gives very reasonable correlation also.

The effects of distorting the mesh have also been considered to a limited extent. Results have been obtained for the relatively coarse meshes shown in Figure 14. Calculated stresses and displacements are presented as a function of aspect ratio and compared to the elasticity solutions in Table 4. As expected, the values are not as accurately determined as are those obtained via the regular meshes. Distortion of the mesh has a much more dramatic effect upon the calculated transverse shear stresses than upon the calculated in-plane stresses and displacements. Since the transverse stresses are based on equilibrium considerations, it seems the mesh must be refined enough to reasonably approximate equilibrium. This is especially apparent in comparing results obtained for mesh A to those obtained for mesh C. In each of these cases, elements having a taper ratio of 2 to 1 are utilized. Mesh C gives significantly improved transverse stresses, however, because the mesh is fine enough to better represent the loading distribution.

Simply Supported Rectangular Plate(0 /90 /0) Sine Load, Material II

Orthotropic layers have the same orientation as in the previous example. The plate has dimensions $a \times b$, where b is three times a . Solutions have been obtained for aspect ratios ($S = a/h$) ranging from 4 to 100. Transverse shear stress variation σ_{yz} at coordinates $(a/2, 0)$ is given in Figure 15 for an aspect ratio $S = 4$. Comparison is made to both elasticity and CPT solutions. A full range of results are presented in Table 5 and compared to those obtained via elasticity

[18] and to those obtained by Reddy [19] in a recent finite element formulation. Correlation with elasticity is quite good, particularly for aspect ratios of 10 and above, and appear to be more accurate than those obtained with the alternate finite element solution.

Simply Supported Square Plate (0 /90 /90 /0) Sine Load, Material II

The laminate geometry consists of outer layers with fibers parallel to the x axis and inner layers with fibers parallel to the y axis. The plate has planar dimension $a \times a$ and total thickness h . Stress and displacement results are presented in Table 6 for aspect ratios ranging from 4 to 100. Similar results are given in Table 6.1 based on the QD formulation. Results are compared to both elasticity and to other finite element results. Again, the computed values are in excellent agreement with elasticity [20] for moderately thick to thin geometries and are more accurate than, the compared to numerical results.

Solutions also have been obtained for the present geometry on the basis of reduced vs. full integration. This comparison is demonstrated in Figures 15 and 17 by giving percent error in calculated values vs. aspect ratio. It is apparent that reduced integration is particularly needed to minimize errors in calculated transverse stresses and, furthermore, solution validity over a wide range of laminate geometries is demonstrated.

Analysis of the geometry of the structure

To assess the effects of finite element formulations, aspect ratio, support conditions and the lamina stacking sequences on the fundamental natural frequencies of composite plates, the problems

listed in Table 7 are considered [21]

The non-dimensionalized fundamental frequency for the cross-ply laminate of Problem 1 versus aspect ratios is given in Table 8. As can be seen, all three elements predict frequencies that are in excellent agreement with the closed form solutions obtained by Reddy [22].

The effects of higher order terms in the displacement based finite element formulations are investigated for Problem 2. Here, the performances of QHD40 and QHD28 (with higher order terms locked) are compared to elements STPD1 and STPD3 of [23] with linear and cubic variations through the thickness respectively. The results are summarized in Table 9. The normalized fundamental frequencies of Problem 3 are displayed in Figure 18. Note that the non-dimensionalized fundamental frequency increases as the angle of orientation is increased for both symmetric and antisymmetric angle-ply square plates. This observation is in excellent agreement with Reddy's [22] antisymmetric laminate. In Figure 19, a decrease in the fundamental frequency is observed as the angle of orientation is increased for the angle-ply, cantilever, rectangular and square plates of Problem 4. The difference between Figures 18 and 19 are attributed primarily to the different support conditions.

Further investigations, Problem 5, of angle-ply laminates are summarized in Table 10. The stacking sequences of reference [24] are used to illustrate their effects on the fundamental frequency calculations. The numbers within parenthesis are calculated by Crawley [24, 25].

Shown in Figure 20 is the variation of the non-dimensionalized fundamental frequency for cylindrical bending problem, as calculated via the QD formulation and the classical plate theory. For comparison purposes, the frequencies are normalized with respect to the classical plate theory results.

Transient Response Calculations

Element performance has been evaluated with respect to predicting linear-transient response. Both displacements and stresses have been determined for a variety of laminated plate geometries subjected to instantaneously applied pressure loading. These results have been compared to those obtained via both CPT and a shear deformable theory (SDT) [26]. Typical results are presented in Figures 21 and 22 for a (0/90) square plate [27]. In this example, the plate is quite thick in that it has an aspect ratio of 5.

II.2. TASK II: Incorporate Damage Mechanisms into Dynamic Response Formulation

The literature survey [28-63] performed has been quite helpful in terms of delineating the viable approaches to including damage mechanisms in the analysis. Relevant failure modes of interest include those listed below

- (i) fiber fracture
- (ii) fiber-matrix debonding
- (iii) matrix cracking (parallel and transverse to fibers)
- (iv) delamination

Several smooth failure criteria, e.g., [64-67] have been developed in recent years to represent the failure of composites. These criteria,

to varying degrees, can predict "failure" but do not identify a particular mode of failure. In performing incremental "damage" analysis, it is essential to both predict failure and to characterize it, e.g., do fibers rupture, does delamination occur, etc. The computational approach must, therefore, differentiate between viable failure modes and appropriately alter the constitutive equations on an incremental basis. This can be accomplished by implementing a piecewise smooth failure criteria, e.g., [28] in the finite element formulation. The general failure criteria is then comprised of m separate inequalities of the form

$$F_j(\sigma) < 1 \quad ; \quad j = 1, 2, \dots, m$$

at the layer level within each element. These criteria can differentiate between (i) tensile and compressive fiber failure, (ii) tensile and compressive matrix failure and (iii) delamination at layer interfaces.

As progressive damage occurs throughout incremental loading (whether) it be static or dynamic), it is essential that violation of failure criteria inequalities be reflected in modification of the material properties. This can be achieved by including damage state variables [47] in the constitutive equations to reflect "stiffness reduction." These equations can be represented as

$$\sigma = [D][\epsilon]$$

where $[D]$ represents the material matrix and $[\epsilon]$ contains the damage state variables. The latter provide the basis for changing the D_{ij}

terms based upon the extent to which the failure criteria are violated.

In conjunction with the above it is essential to perform equilibrium iterations within each analysis increment. This is required to assure that stress redistribution is properly accounted for as damage progresses.

The relevant failure nodes of interest and appropriate criteria used in the incremental analysis are listed in Table II.

Damage Initiation Calculations:

The damage histories of graphite/epoxy (T300/5208) composite laminates under in-plane load increments are presented for selected models [68]. The ability to differentiate between relevant failure/damage modes is illustrated in Figures 23 and 24.

II.3.3 TASK III: Correlation of Formulated Response Model with Experimental Data

Some quantitative data relating to the impact damage of composite specimens has been assembled [69-76]. It will be utilized along with any additional data obtained to perform analysis/test correlations. Since the nonlinear formulation including damage effects is not complete, no use of the test data has been made to this point.

III. REFERENCES

1. Whitney, J.M., "The Effects of Transverse Shear Deformation on the Bending of Laminated Plates," *J. Composite Materials*, 1969, Vol. 3, p. 534.
2. Pagano, N.J., "Stress Fields in Composite Laminates," *Int. J. Solids and Structures*, 1978, Vol. 14, p. 385-400.
3. Barker, R.M., Fu-Tien Lin, Dana, J.R., "Three Dimensional Finite Element Analysis of Laminated Composites," *Computers & Structures*, 1972 Vol. 2, p. 1013-1029.
4. Pian, T.H.H., and Tong, P., "Finite Element Methods in Continuum Mechanics," *Advances in Applied Mechanics*, 1972, Vol. 2, p. 1-58.
5. Reddy, J.N., "Bending of Laminated Anisotropic Shells by a Shear Deformable Finite Element," *Fiber Science and Technology*, 1982, Vol. 2, p. 9-24.
6. Pagano, N.J., "On the Calculation of Interlaminar Normal Stress in Composite Laminates," *J. of Composite Materials*, 1974, Vol. 8, p. 65-81.
7. Spilker, R.L., Chow, S.C. and Orringer, O., "Alternate Hybrid-Stress Elements for Analysis of Multilayer Composite Plates," *J. Composite Materials*, 1977, Vol. 11, p. 51-70.
8. Mau, S.T., Tong, P., and Pian, T.H.H., "Finite Element Solutions for Laminated Thick Plates," *J. Composite Materials*, 1972, Vol. 6, p.304-305.
9. Pagano, N.J., "Exact Solutions for Composite Laminates in Cylindrical Bending," *J. Composite Materials*, 1969, Vol. 3, p. 398-411.
10. Pryor, C.W., and Barker, R.M., "Finite Element Analysis Including

- Transverse Shear Effects for Application to Laminated Plates," *AIAA Journal*, 1971, p. 912-917.
11. Whitney, J.M., and Leissa, A.W., "Analysis of Heterogeneous Anisotropic Plates," *Journal of Applied Mechanics*, 1969, Vol 36, p. 261-266.
 12. Giri, J., and Simitzes, G.K., "Deflection Response of General Laminated Composite Plates to In-Plane and Transverse Loads," *Fiber Science and Technology*, 1980, Vol. 13, p. 225-242.
 13. Whittaker, E. and Robinson, G., The Calculus of Observations, Blackie and Son, Limited, Glasgow, 1944.
 14. O.C. Zienkiewicz, R.L. Taylor and J.M. Too, 'Reduced Integration Technique in General Analysis of Plates & Shells', *Int. J. Num. Meth. Engrg.* 3, 275-290 (1971).
 15. E.D.L. Pugh, E. Hinton, and O.C. Zienkiewicz, 'A Study of Quadrilateral Plate Bending Elements with Reduced Integration' *Int. J. Num. Meth. Engrg.* 12, 1059-1079 (1978).
 16. T.J.R. Hughes, M. Cohen and M. Haroun, 'Reduced and Selective Integration Techniques in the Finite Element Analysis of Plates', *Intl. Engrg. Res.* 46, 203-222 (1978).
 17. Ted Belytschki and Chen-Shyh Tsay, 'A Stabilization Procedure for the Quadrilateral Plate Element with One-Point Quadrature', *Int. J. Num. Meth. Engrg.* 19, 405-419 (1983).
 18. N.J. Pagano, 'Exact Solutions for Rectangular Bidirectional Composites and Sandwich Plates', *J. Comp. Mat'ls.* 4, 20-34 (1970).
 19. J.N. Reddy, 'A Penalty Plate-Bending Element for the Analysis of Laminated Anisotropic Composite Plates', *J. Comp. Mat'ls.* 15, 1187-1206 (1980)

20. N.J. Pagano and S.J. Hatfield, 'Elastic Behavior of Multilayered Bidirectional Composites', *AIAA Jnl.* 10, 931-933 (1972).
21. O.O. Ochoa, J.J. Engblom, R.T. Tucker, "A Study of Effects of Kinematic and Material Characteristics of the Fundamental Frequency Calculations of Composite Plates," *Int. J. Num. Meth. Engrg.*, Accepted for Publication.
22. J.N. Reddy, and W.C. Chao, 'A Comparison of Closed-Form and Finite Element Solutions of Thick Laminated Anisotropic rectangular Plates.' *Nuclear Engineering and Design* 64, 153-167. 1981
23. J.N. Reddy 'An Accurate Prediction of Natural Frequencies of Laminated Plates by Higher Order Theory', *Advances in Aerospace Structures and Materials* ed. Uman Yuceoglu, Winter Annual Meeting of ASME, Boston, Massachusetts. 1983
24. E.F. Crawley and J. Dugundji, 'Frequency determination and Non-Dimensionalization for Composite Cantilever Plates' 72, 1-10. 1980. *Journal of Sound and Vibration*.
25. E.F. Crawley 'The Natural Modes of Graphite/Epoxy Catilever Plates and Shells', catilever plates and shells. *J. Composite Materials* 13, 195-205.
26. J.N. Reddy, "On the Solutions to Forced Motion on Rectangular Composite Plates, " , *Journal of Applied Mech.* 49, 403-408, 1982.
27. N.P. Fox, "Transient Response of Composite Plates Due to Transverse Loading", TAMU Technical Report, 1984.
28. Hashin, Z., "Failure Criteria for Unidirectional Fiber Composites," *J. Applied Mechanics* , Vol. 47, 1980, p.329.
29. Lee. J.D., "Three Dimensional Finite Element Analysis of Damage

- Accumulation in Composite Laminate," *Computers & Structures*, Vol. 15, No. 3, 1982, p. 335.
30. Rosen, B.W., "Failure of Fiber Composite Laminates," *Mechanics of Composite Materials*, p. 105.
31. Greszczuk, L.B., "Microbuckling of Lamina-Reinforced Composites," *Composite Materials: Testing and Design (third conference)*, ASTM STP 546, American Society for Testing and Materials, 1974, p. 5.
32. Whitney, J.M. and Browning, C.E., "On Interlaminar Beam Experiments for Composite Materials," *Proceedings of the V International Congress on Experimental Mechanics*, 1983, p.97
33. Soni, S.R. and Pagano, N.J., "Elastic Response of Composite Laminates," *Mechanics of Composite Materials*, p.227.
34. Whitcomb, J.D., "Finite Element Analysis of Instability Related Delamination Growth," *J. Composite Materials*, Vol.17, 1964, p.217.
35. Biot, M.A., "Theory of Stability of Periodic Multilayered Continua," *Quarterly Journal of Mechanics and Applied Mathematics*, Vol. 17, 1964.
36. Simites, G.J., et.al., "Effect of Delamination on Axially-Loaded Laminated Plates," AIAA, 1984, p.351.
37. Yin, W.L., et.al., "Ultimate Axial Load Capacity of a Delaminated Plate," AIAA, 1984. p. 159.
38. Lee, J.D., "Three Dimensional Finite Element Analysis of Layered Fiber-Reinforced Composite Materials," *Computers & Structures*, Vol. 12, 1980, p.319.
39. Hahn, H.T. and Williams, J.G., "Compression Failure Mechanisms in Unidirectional Composites," Unpublished.

40. Hahn, H.T. and Tsai, S.W., "On the Behavior of Composite Laminates After Initial Failures," *J. Composite Materials*, Vol. 8, 1984, p.288.
41. Sandhu, R.S., et.al., "Modeling of the Failure Process in Notched Laminates," *Mechanics of Composite Materials*, p. 179.
42. Reifsnider, K.L., et.al., "Damage Mechanics and NDE of Composite Laminates," *Mechanics of Composite Materials*, p.399.
43. Soni, S.R., "A New Look at Commonly Used Failure Theories in Composite Laminates," *24th Structures, Structural Dynamics and Materials Conference, A Collection of Technical Papers, AIAA/ASME/ASCE/AHS, Lake Tahoe, 1983*, p.171.
44. Sandhu, R.S., et.al., "Initiation and Accumulation of Damage in Composite Laminates," *Composite Materials: Testing and Design (sixth conference), ASTM STP 787, American Society for Testing and Materials, 1982*, p.163.
45. Nuismer, R.J. and Tan, S.C., "The Role of Matrix Cracking in the Continuum Constitutive Behavior of a Damaged Composite Ply," *Mechanics of Composite Materials*, p.437.
46. Nuismer, R.J., "Continuum Modeling of Damage Accumulation and Ultimate Failure in Fiber Reinforced Laminated Composite Materials," Univ. of Utah, p.55.
47. Nuismer, R.J., "Predicting the Performance and Failure of Multi-directional Polymeric Matrix Composite Laminates: a Combined Micro-Macro Approach," Univ. of Utah, p. 436.
48. Christensen, R.M., "Mechanical Properties of Composite Materials," *Mechanics of Composite Materials*, p.1.

49. Nemat-Nasser, S. and Iwakuma, T., "Finite Elastic-Plastic Deformation of Composites," *Mechanics of Composite Materials*, p.47.
50. Rotem, A. and Hashin, Z., "Failure Modes of Angle Ply Laminates," *J. Composite Materials*, Vol. 9, 1975, p. 191.
51. Reifsnider, K.L., "Characteristic Damage States in Composite Laminates," Virginia Polytechnic Institute, p. 147.
52. Wang, A.S., "Growth Mechanisms of Transverse Cracks and Ply Delamination in Composite Laminates," Drexel Univ., p. 170.
53. Wang, A.S., "Interlaminar Failure in Epoxy Based Composite Laminates," Drexel Univ., p.255.
54. Goree, J.D. and Gross, R.S., "Analysis of a Unidirectional Composite Containing Broken Fibers and Matrix Damage," *Engineering Fracture Mechanics*, Vol. 13, 1979, p. 563.
55. Davis J.G., "Compressive Strength of Fiber-Reinforced Composite Materials," *Composite Reliability*, ASTM STP 580, American Society for Testing and Materials, 1975, p.364.
56. Tsai, S.W., "A Survey of Microscopic Failure Criteria for Composite Materials," *J. Reinforced Plastics and Composites*, Vol. 3, 1984, p. 40.
57. Konish, H.J., et.al., "Experimental Investigation of Fracture in an Advanced Fiber Composite," *J. Composite Materials*, Vol. 6, 1972, p. 114.
58. Chang, F.H., et. al., "Real-Time Characterization of Damage Growth in Graphite/Epoxy Laminates," *J. Composite Materials*, Vol.10, 1976, p. 182.
59. Petit, P.H. and Waddoups, M.E., "A Method of Predicting the

- Nonlinear Behavior of Laminated Composites," *J. Composite Materials*, Vol. 3, 1969, p. 2.
60. Pagano, N.J. and Pipes, R.B., "The Influence of Stacking Sequence on Laminate Strength," *J. Composite Materials*, Vol. 5, 1971, p. 50
61. Puppo, A.H. and Evensen, H.A., "Strength of Anisotropic Materials Under Combined Stresses," *AIAA Journal*, Vol. 10, 1972, p. 468.
62. Hahn, H.T., "Nonlinear Behavior of Laminated Composites," *J. Composite Materials*, Vol. 7, 1973, p. 257.
63. Dharani, L.R. and Goree, J.G., "Analysis of a Hybrid, Uni-directional Laminate with Damage," *Mechanics of Composite Materials*, p. 165.
64. Hill, R., "A Theory of the Yielding and Plastic Flow of Anisotropic Materials," *Proceedings of the Royal Society, London*, 1948, Series A, Vol. 193, p. 281-290.
65. Tsai, S.W., "Strength Characteristics of Composite Materials, NASA CR-224, 1965.
66. Hoffman, I., "The Brittle Strength of Orthotropic Materials," *J. Composite Materials*, 1967, Vol. 1, p. 200-206.
67. Tsai, S.W. and Wu, E.M., "A General Theory of Strength for Anisotropic Materials," *J. Composite Materials*, 1971, Vol. 5, p. 58-81.
68. M.C. Kilpatrick, "The Inclusion of Damage Effects in an Incremental Finite Element Analysis of Composite Plates," TAMU M.S. Thesis, 1984.
69. Novak, R.C., "Composite for Blade Development Resin Matrix Composites," United Technologies Report R76-214278-1, 1976.

70. Prewo, K.M., "Composite for Blade Development Metal Matrix Composites," United Technologies Report R76-214278-2, 1976.
71. Veltri, R.D., and Prewo, K.M., "The Slow Indention Testing of Simulated Blade Specimens," United Technologies Report, R77-216956-1, 1977.
72. Daniel, I.M. and Leber, T., "Wave Propagation in Fiber Composite Laminates," NASA-CR-135086, 1977.
73. Engblom, J.J., "Coupled Fluid/Structure Response Predictions for Soft Body Impact of Airfoil Configurations," ASME - Emerging Technologies in Aerospace Structures, Design, Structural Dynamics and Materials, 1980, p. 209-223.
74. Bertke, R.S., "Local Leading Edge Damage from Hard Particle and Soft Body Impacts (Task IV B)," AFWAL-TR-82-2044, 1982.
75. Bertke, R.S., "Structural Element and Real Blade Impact Testing," Univ. of Dayton Report UDRI-TR-82-02, 1982.
76. Storace, A.F., "Foreign Object Impact Design Criteria," General Electric Company Interim Report for Contract #F33615-77-C-5221, 1982.

IV. TABLES AND FIGURES

Table 1. Spurious Zero Energy Modes of the QHD Family

	Quadrature Order	Number of Zero Eigenvalues	Number of Spurious Modes
QHD40	3x3 with 2x2 for transverse shear terms	6	0
QHD28	2x2 with 1x1 for transverse shear terms	9	3
QHD20	2x2 with 1x1 for transverse shear terms	8	2

TABLE 2

Material Properties used in the sample problems

MATERIAL	E_1/E_2	G_{12}/E_2	G_{23}/E_2	γ	$\rho \frac{\text{lb-sec}^2}{\text{in}^4}$
I	40	0.60	0.5	0.25	$.7124 \times 10^{-4}$
II	25	0.50	0.2	0.25	$.7124 \times 10^{-4}$
III	11.6	0.41	0.14	0.25	$.1425 \times 10^{-3}$
IV	25	--	--	0.25	$.7124 \times 10^{-4}$

TABLE 3

NUMERICAL STRESSES AND DISPLACEMENTS FOR SIMPLY SUPPORTED SQUARE 0-90-0 PLATE WITH SINUSOIDAL LOAD

S	Approach	$\bar{\sigma}_x$ $(\frac{a}{2}, \frac{a}{2}, \pm \frac{h}{2})$	\bar{v}_y $(\frac{a}{2}, \frac{a}{2}, \pm \frac{h}{6})$	$\bar{\sigma}_{xy}$ $(0, 0, \pm \frac{h}{2})$	$\bar{\sigma}_{xz}$ $(0, \frac{a}{2}, 0)$	$\bar{\sigma}_{yz}$ $(\frac{a}{2}, 0, 0)$
4	FEM (2x2 Mesh)	.414	.598	.0465	.296	.238
	FEM (6x6 Mesh)	.391	.572	.0448	.308	.251
	Elasticity	.755	.556	.0505	.282	.217
10	FEM (2x2 Mesh)	.529	.292	.0289	.352	.123
	FEM (6x6 Mesh)	.500	.279	.0280	.369	.130
	Elasticity	.590	.288	.0289	.357	.123
20	FEM (2x2 Mesh)	.560	.206	.0240	.367	.0910
	FEM (6x6 Mesh)	.531	.189	.0233	.387	.0954
	Elasticity	.552	.210	.0234	.385	.0938
50	FEM (2x2 Mesh)	.567	.178	.0226	.374	.0812
	FEM (6x6 Mesh)	.541	.164	.0217	.392	.0843
	Elasticity	.541	.185	.0216	.393	.0842
100	FEM (2x2 Mesh)	.566	.174	.0224	.375	.0803
	FEM (6x6 Mesh)	.542	.167	.0215	.393	.0827
	Elasticity	.539	.181	.0213	.395	.0828
	GPT	.539	.180	.0213	.395	.0823

TABLE 3.1

S	Approach	$\bar{\sigma}_x$ $(\frac{a}{2}, \frac{a}{2}, \pm\frac{h}{2})$	$\bar{\sigma}_y$ $(\frac{a}{2}, \frac{a}{2}, \pm\frac{h}{6})$	$\bar{\sigma}_{xy}$ $(0, 0, \pm\frac{h}{2})$	$\bar{\sigma}_{xz}$ $(0, \frac{a}{2}, 0)$	$\bar{\sigma}_{yz}$ $(\frac{a}{2}, 0, 0)$
4	FEM (3x3 Mesh)	.399	.562	.0513	.372	.304
	FEM (6x6 Mesh)	.392	.543	.0463	.357	.280
	Elasticity	.755	.556	.0505	.282	.217
10	FEM (3x3 Mesh)	.514	.246	.0299	.406	.175
	FEM (6x6 Mesh)	.502	.270	.0284	.387	.142
	Elasticity	.590	.288	.0289	.357	.123
20	FEM (3x3 Mesh)	.547	.157	.0245	.418	.141
	FEM (6x6 Mesh)	.533	.186	.0234	.398	.107
	Elasticity	.552	.210	.0234	.385	.0938
50	FEM (3x3 Mesh)	.558	.128	.0227	.423	.130
	FEM (6x6 Mesh)	.543	.159	.0219	.402	.0961
	Elasticity	.541	.185	.0216	.393	.0842
100	FEM (3x3 Mesh)	.559	.123	.0225	.423	.128
	FEM (6x6 Mesh)	.544	.155	.0216	.403	.0944
	Elasticity	.539	.181	.0213	.395	.0828
	CPT	.539	.180	.0213	.395	.0823

TABLE 4
 STRESS COMPONENTS IN A PLATE WITH SINUSOIDAL LOAD (DISTORTED MESHES)

s	Approach	$\bar{\sigma}_x$ $(\frac{a}{2}, \frac{a}{2}, \frac{h}{4})$	$\bar{\sigma}_y$ $(\frac{a}{2}, \frac{a}{2}, \frac{h}{4})$	$\bar{\sigma}_{xy}$ $(0, 0, \frac{h}{2})$	$\bar{\sigma}_{xz}$ $(0, \frac{a}{2}, 0)$	$\bar{\sigma}_{yz}$ $(\frac{a}{2}, 0, 0,)$	$\bar{\tau}$ $(\frac{a}{2}, \frac{a}{2}, 0)$
4	Mesh A	.409	.620	.0525	.128	.122	2.709
	Mesh B	.393	.573	.0485	.254	.206	2.473
	Mesh C	.402	.596	.0472	.290	.229	2.587
	Elasticity	.755	.556	.0505	.282	.217	--
10	Mesh A	.539	.292	.0344	.141	.0686	.866
	Mesh B	.502	.279	.0300	.293	.107	.812
	Mesh C	.530	.286	.0290	.357	.114	.839
	Elasticity	.590	.288	.0289	.357	.123	--
20	Mesh A	.574	.198	.0297	.153	.0552	.545
	Mesh B	.531	.199	.0248	.303	.0792	.529
	Mesh C	.571	.198	.0239	.378	.0880	.539
	Elasticity	.552	.210	.0234	.385	.0938	--
50	Mesh A	.585	.174	.0300	.180	.0516	.443
	Mesh B	.535	.178	.0226	.304	.0701	.445
	Mesh C	.587	.177	.0221	.378	.0955	.449
	Elasticity	.541	.185	.0216	.393	.0842	--
100	Mesh A	.591	.190	.0312	.200	.0363	.418
	Mesh B	.531	.176	.0215	.302	.0689	.432
	Mesh C	.596	.180	.0212	.359	.112	.433
	Elasticity	.539	.181	.0213	.395	.0828	--
	GPT	.539	.180	.0213	.395	.0823	

TABLE 5

NORMALIZED STRESSES AND DISPLACEMENTS FOR SIMPLY SUPPORTED RECTANGULAR 0-90-0 PLATE WITH SINUSOIDAL LOAD

S	Approach	$\bar{\sigma}_x$ $(\frac{a}{2}, \frac{b}{2}, \frac{h}{2})$	$\bar{\sigma}_y$ $(\frac{a}{2}, \frac{b}{2}, \frac{h}{2})$	$\bar{\sigma}_{xy}$ $(0, 0, \frac{h}{2})$	$\bar{\sigma}_{xz}$ $(0, \frac{b}{2}, 0)$	$\bar{\sigma}_{yz}$ $(\frac{a}{2}, 0, 0)$	\bar{w} $(\frac{a}{2}, \frac{b}{2}, 0)$
4	FEM (2x2 Mesh)	.657	.130	.0296	.410	.0357	3.55
	FEM (6x6 Mesh)	.612	.126	.0284	.431	.0391	3.58
	FEM (Reddy)	--	--	--	--	--	--
	Elasticity	.726	.119	.0281	.420	.0334	2.82
10	FEM (2x2 Mesh)	.669	.0431	.0125	.414	.0143	.995
	FEM (6x6 Mesh)	.625	.0421	.0121	.436	.0160	1.00
	FEM (Reddy)	.603	.0364	.0102	--	--	.802
	Elasticity	.725	.0435	.0123	.420	.0152	.919
20	FEM (2x2 Mesh)	.666	.0286	.00959	.415	.0112	.625
	FEM (6x6 Mesh)	.628	.0278	.00928	.437	.0121	.629
	FEM (Reddy)	.605	.0276	.00986	--	--	.578
	Elasticity	.650	.0299	.0093	.434	.0119	.610
50	FEM (2x2 Mesh)	.659	.0252	.00878	.416	.0113	.521
	FEM (6x6 Mesh)	.629	.0237	.00848	.437	.0110	.524
	FEM (Reddy)	.604	.0251	.0081	--	--	.515
	Elasticity	.628	.0259	.0084	.439	.0110	.520
100	FEM (2x2 Mesh)	.657	.0259	.00856	.416	.0127	.507
	FEM (6x6 Mesh)	.628	.0231	.00837	.437	.0108	.509
	FEM (Reddy)	.603	.0253	.0080	--	--	.506
	Elasticity	.624	.0253	.0083	.439	.0108	.508
	CPT	.623	.0252	.0083	.440	.0108	.503

TABLE 6

NORMALIZED STRESSES AND DISPLACEMENTS FOR SIMPLY SUPPORTED SQUARE 0-90-90-0 PLATE WITH SINUSOIDAL LOAD

S	Approach	\bar{v}_x $(\frac{a}{2}, \frac{a}{2}, \frac{h}{2})$	\bar{v}_y $(\frac{a}{2}, \frac{a}{2}, \frac{h}{4})$	$\bar{\sigma}_{xy}$ $(0, 0, \frac{h}{2})$	$\bar{\sigma}_{xz}$ $(0, \frac{a}{2}, 0)$	$\bar{\sigma}_{yz}$ $(\frac{a}{2}, 0, 0)$	$\bar{\omega}$ $(\frac{a}{2}, \frac{a}{2}, 0)$
4	FEM (2x2 Mesh)	.409	.646	.0336	.245	.286	5.166
	FEM (6x6 Mesh)	.387	.618	.0326	.256	.302	5.195
	FEM (Reddy)	--	--	--	--	--	--
	Elasticity	.720	.666	.0467	.270	.292	4.491
10	FEM (2x2 Mesh)	.516	.406	.0261	.294	.185	1.762
	FEM (6x6 Mesh)	.488	.388	.0253	.309	.195	1.771
	FEM (Reddy)	.484	.350	.0234	--	--	1.534
	Elasticity	.559	.403	.0276	.301	.196	1.709
20	FEM (2x2 Mesh)	.555	.316	.0233	.313	.147	1.197
	FEM (6x6 Mesh)	.526	.302	.0226	.329	.155	1.203
	FEM (Reddy)	.511	.287	.0214	--	--	1.136
	Elasticity	.543	.309	.0230	.328	.156	1.189
50	FEM (2x2 Mesh)	.566	.283	.0224	.320	.135	1.029
	FEM (6x6 Mesh)	.540	.271	.0216	.336	.140	1.034
	FEM (Reddy)	.520	.265	.0207	--	--	1.019
	Elasticity	.539	.276	.0216	.337	.141	1.031
100	FEM (2x2 Mesh)	.566	.278	.0223	.322	.133	1.003
	FEM (6x6 Mesh)	.542	.266	.0215	.337	.138	1.010
	FEM (Reddy)	.523	.263	.0207	--	--	1.005
	Elasticity	.539	.271	.0214	.339	.139	1.008
	CPT	.539	.269	.0213	.339	.138	1.

TABLE 6.1

h	Approach	\bar{v}_x $(\frac{a}{2}, \frac{a}{2}, \frac{h}{4})$	\bar{v}_y $(\frac{a}{2}, \frac{a}{2}, \frac{h}{4})$	\bar{v}_{xy} $(0, 0, \frac{h}{2})$	\bar{v}_{xz} $(0, \frac{a}{2}, 0)$	\bar{v}_{yz} $(\frac{a}{2}, 0, 0)$	\bar{v} $(\frac{a}{2}, \frac{a}{2}, 0)$
4	FEM (2x2 Mesh)	.394	.617	.0388	.314	.361	5.392
	FEM (6x6 Mesh)	.387	.615	.0341	.300	.336	5.245
	FEM (Reddy)	--	--	---	--	--	---
	Elasticity	.720	.666	.0467	.270	.292	4.491
10	FEM (2x2 Mesh)	.502	.372	.0271	.342	.239	1.844
	FEM (6x6 Mesh)	.490	.382	.0257	.325	.209	1.790
	FEM (Reddy)	.484	.350	.0234	--	--	1.534
	Elasticity	.559	.403	.0276	.301	.196	1.709
20	FEM (2x2 Mesh)	.542	.280	.0237	.358	.198	1.254
	FEM (6x6 Mesh)	.528	.295	.0228	.339	.167	1.216
	FEM (Reddy)	.511	.287	.0214	--	--	1.136
	Elasticity	.543	.309	.0230	.328	.156	1.189
50	FEM (2x2 Mesh)	.556	.247	.0225	.364	.183	1.078
	FEM (6x6 Mesh)	.542	.264	.0217	.345	.152	1.045
	FEM (Reddy)	.520	.265	.0207	--	--	1.019
	Elasticity	.539	.276	.0216	.337	.141	1.031
100	FEM (2x2 Mesh)	.559	.242	.0223	.365	.181	1.052
	FEM (6x6 Mesh)	.544	.259	.0216	.346	.146	1.021
	FEM (Reddy)	.523	.263	.0207	--	--	1.005
	Elasticity	.539	.271	.0214	.339	.139	1.008
	CPT	.539	.269	.0213	.339	.138	1.000

TABLE 7
Summary of Numerical Examples

Problem #'s	Element Type	Plate Geometry	Plate Support Conditions	Material Type	Plate Aspect Ratio	Lamina Stacking Sequence
1	QHD28 QHD40 QD32	Square (a/b=1)	Simply Supported	II	2, ..., 100	0°/90°/90°/0°
2	QHC40 QHD28 (with i_x and i_y locked)	Square (a/b=1)	Simply Supported	I	5, 10, 100	0°/90°/0°
3	QD32	Square (a/b=1)	Simply Supported	I II	10	0°/0°/0°/0° and 0°/0°/0°/0°
4	QD32	Rectangular (a/b=2) Square (a/b=1)	Cantilever	III	10	0°/0°/0°/0°
5	QHD40	Rectangular (a/b=2)	Cantilever	III	2, ..., 144	(±45, ±45) [0 ₂ , ±30] _s [0, ±45, 90] _s
6	QD32	Narrow Rectangular Strip	Cylindrical Bending	I IV	2, ..., 100	0°/90°/0°

TABLE 8

Nondimensionalized Fundamental Frequencies of Simply Supported,
Square, Cross-ply Plate of Problem 1.

$$\bar{\omega} = \omega \frac{a^2}{t} \sqrt{\frac{\rho}{E_2}}$$

Aspect Ratio	Finite	Element	Solution	Closed Form Solution Preference [4]
	QHD28	QHD40	QD32	
2	5.860	5.525	5.824	5.500
4	9.780	9.757	9.706	9.359
10	15.440	15.340	15.276	15.145
20	17.850	17.719	17.628	17.665
25	18.246	18.103	18.006	18.093
100	18.964	18.805	18.704	18.733

TABLE 9

The Effects of Linear (z), Quadratic (z^2) and Cubic (z^3) Variations Through-the-Thickness on Fundamental Frequencies of

Problem 2. $\left(\bar{\omega} = \omega \frac{a^2}{t} \sqrt{\frac{\rho}{E_2}}\right)$

Aspect Ratio a/t	Displacement Field Model					Classical Plate Theory
	Linear		Quadratic QHD40	Cubic STPD3	Classical Plate Theory	
	STPD1	QHD28 ($\phi_x = \phi_y = 0$)				
5	8.608	7.551	9.557	8.237	14.501	
10	12.163	11.1	12.869	11.790	15.104	
100	15.183	15.260	15.169	15.175	15.222	

TABLE 10

Nondimensionalized Fundamental Frequency
of Cantilever, Angle Ply Plates of Problem 5

$$\left(\bar{\omega} = \omega \frac{a^2}{t} \sqrt{\frac{\rho}{E_2}} \right)$$

Aspect Ratio a/t	Lamina Stacking Sequence		
	$[\pm 45, \mp 45]_S$	$[0_2, \pm 30]_S$	$[0, \pm 45, 90]_S$
2	1.17	1.72	1.64
5	1.43	2.79	2.47
10	1.53	3.02	2.73
20	1.60	3.31	2.82
24	1.62	3.32	2.83
144	1.68 (1.64)	3.35 (3.35)	2.86 (2.85)

TABLE 1

SELECTED DAMAGE CRITERIA

	FIBER FAILURE		MATRIX FAILURE		DELAMINATION
	TENSILE	COMPRESSIVE	TENSILE	COMPRESSIVE	
HASHIN	$\left(\frac{\sigma_{11}}{C_A}\right)^2 + \left(\frac{\sigma_{12}^2 + \sigma_{13}^2}{\tau_A^2}\right) = 1$	-----	$\left(\frac{\sigma_{22} + C}{C_T}\right)^2 + \frac{\sigma_{23}^2 - \sigma_{22}\sigma_{33}}{\tau_T^2} + \frac{\sigma_{12}^2 + \sigma_{13}^2}{\tau_A^2} = 1$	$\frac{1}{C_T} \left(\left(\frac{\sigma_T^2}{2\tau_T} \right) - 1 \right) (\sigma_{22} + \sigma_{33}) + \frac{1}{4\tau_T^2} (\sigma_{22} + \sigma_{33})^2 + \frac{1}{\tau_T^2} (\sigma_{23}^2 - \sigma_{22}\sigma_{33}) + \frac{1}{\tau_T^2} (\sigma_{12}^2 + \sigma_{13}^2) = 1$	-----
	<p>OR</p> $\sigma_{11} = \sigma_A$	-----	$\sigma_{22} = \sigma_T$	-----	$\frac{\sigma_{33}}{\sigma} = 1$
LEE	$\sigma_{12}^2 + \sigma_{12}^2 = \tau_A^2$	-----	$\sigma_{12}^2 + \sigma_{23}^2 = \tau_T^2$	-----	$\frac{\sigma_{13}^2 + \sigma_{23}^2}{\tau^2} = 1$
GRESZCZUK	-----	(Buckling)	-----	-----	-----
	-----	$\sigma_C = \frac{C_T}{1-k}$	-----	-----	$\left(\frac{\sigma_{33}}{\sigma}\right)^2 + \frac{\sigma_{22} + \sigma_{23}^2}{\tau^2} = 1$

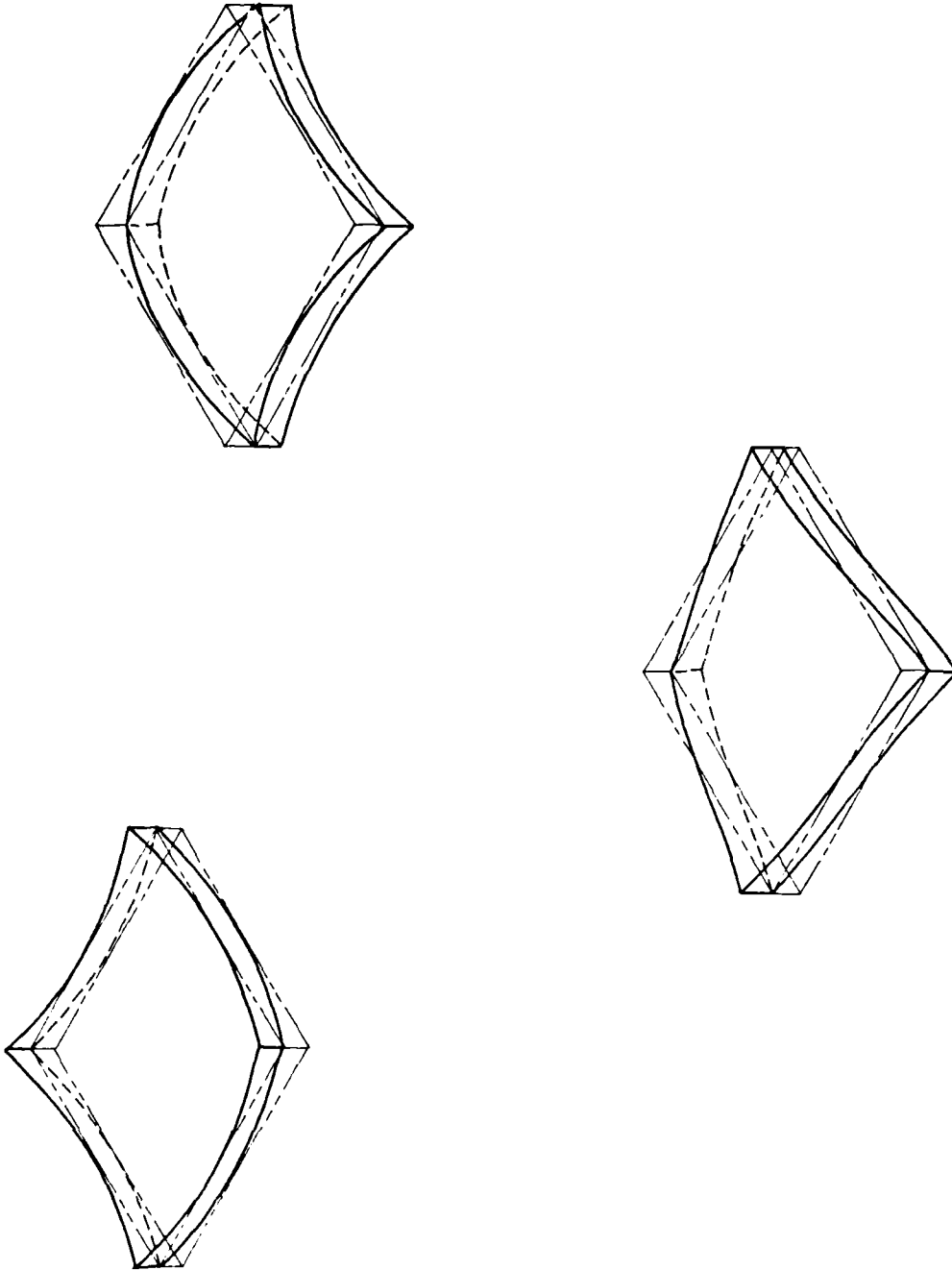


Figure 1: SPURIOUS ZERO ENERGY MODES (QHD28 ELEMENT)

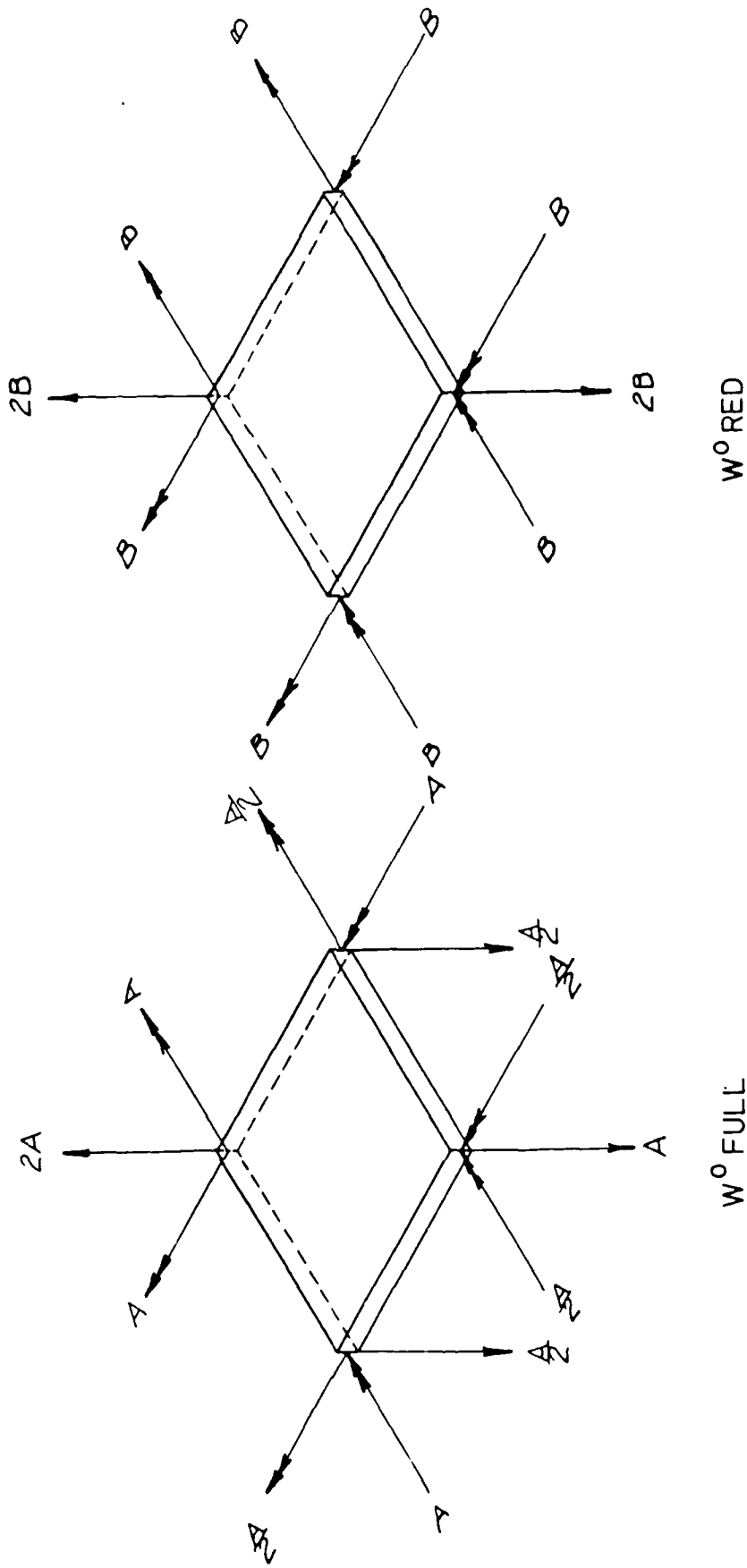


Figure 2: GENERALIZED FORCES

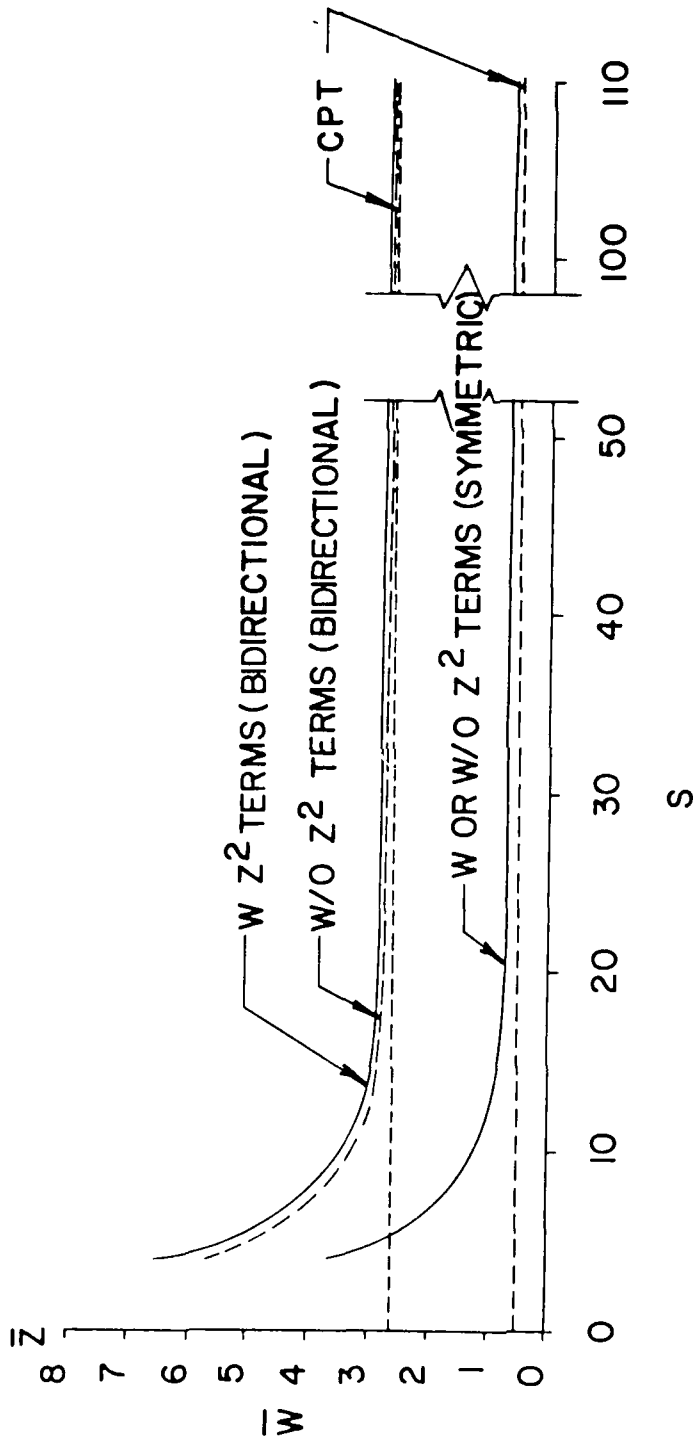


FIGURE 3: NORMALIZED TRANSVERSE DISPLACEMENT VS. ASPECT RATIO FOR CYLINDRICAL BENDING OF BIDIRECTIONAL AND SYMMETRIC 3-PLY LAMINATES

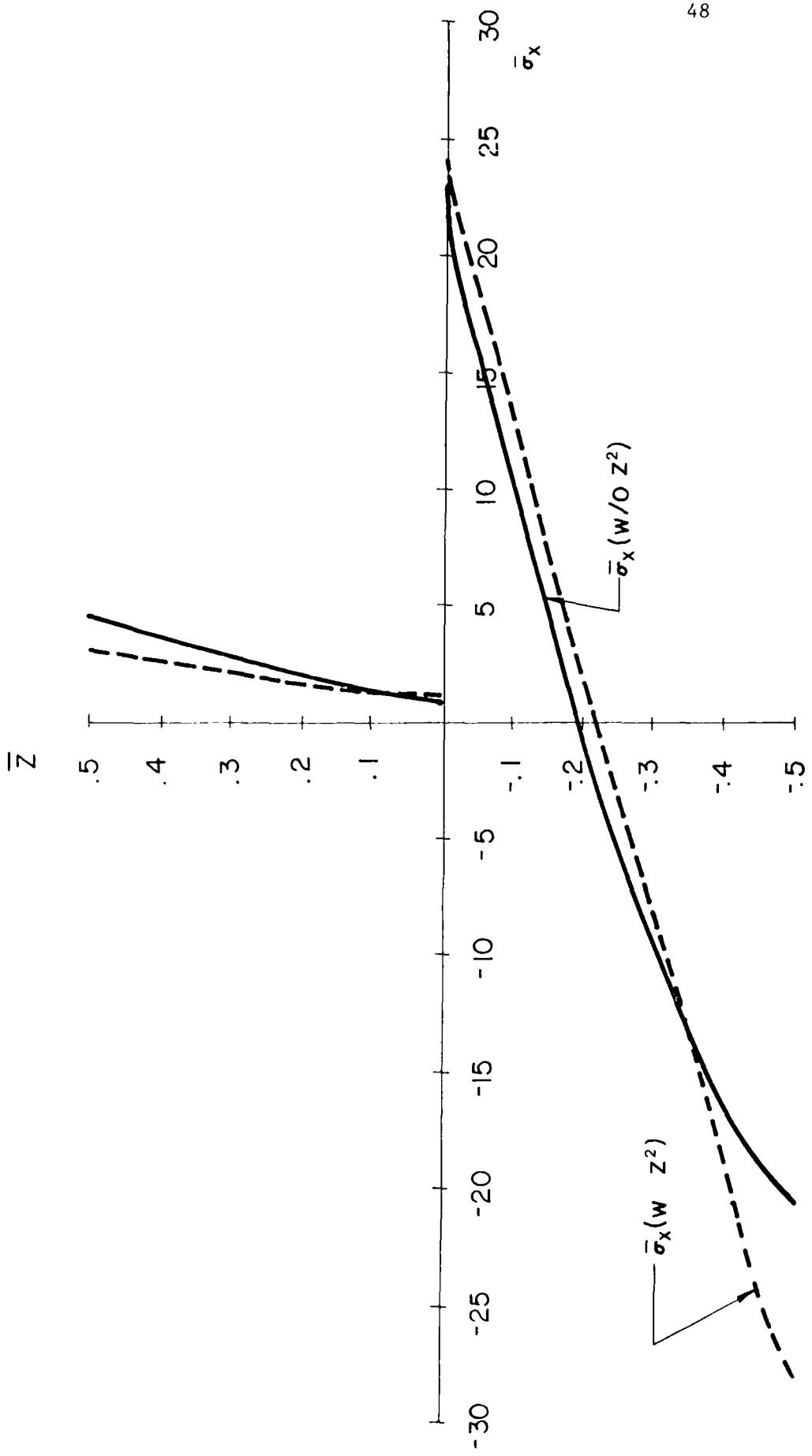


FIGURE 4: NORMALIZED IN-PLANE STRESS FOR CYLINDRICAL BENDING OF BIDIRECTIONAL LAMINATE (S=4)

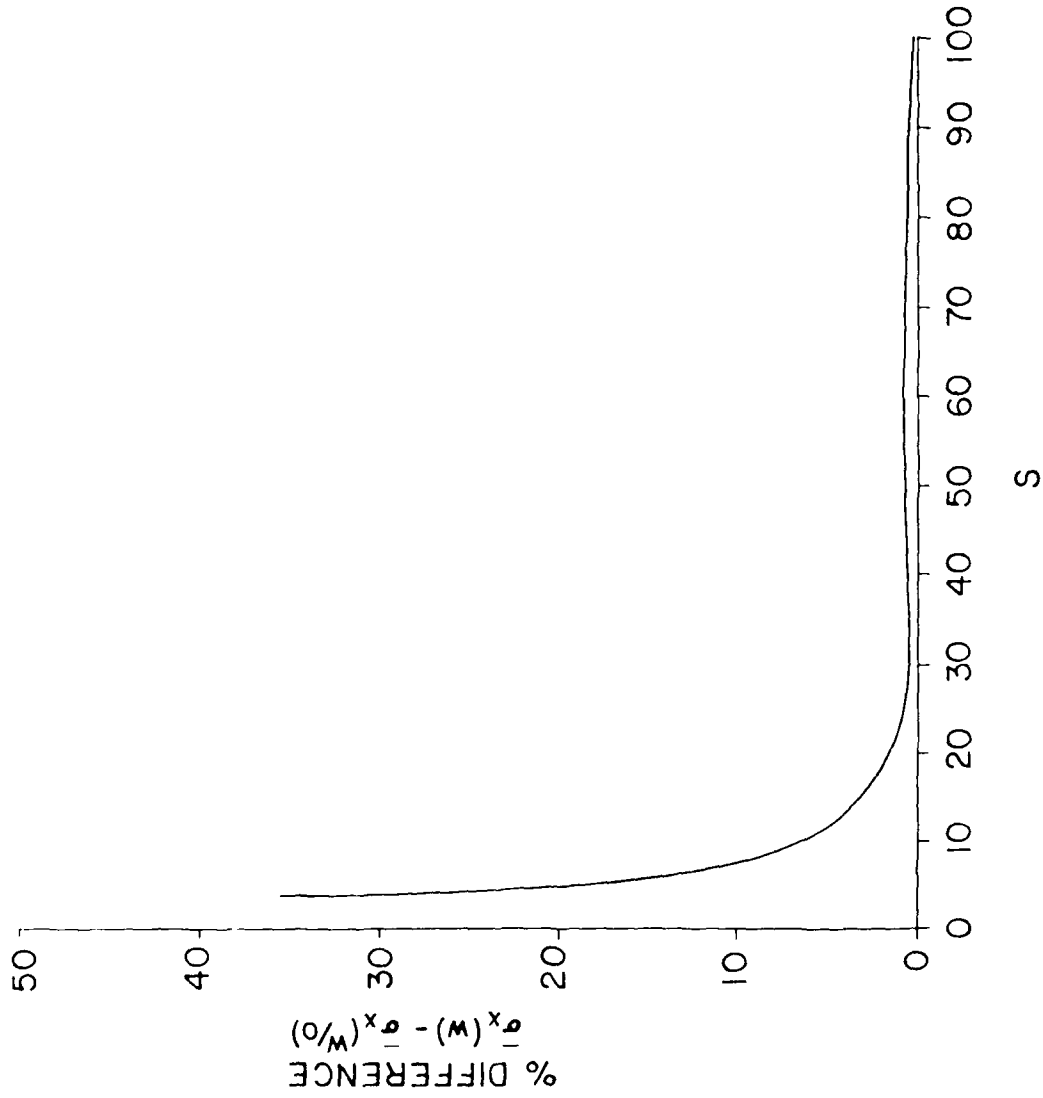


FIGURE 5: NORMALIZED IN-PLANE STRESS VS. ASPECT RATIO FOR CYLINDRICAL BENDING OF BIDIRECTIONAL LAMINATE

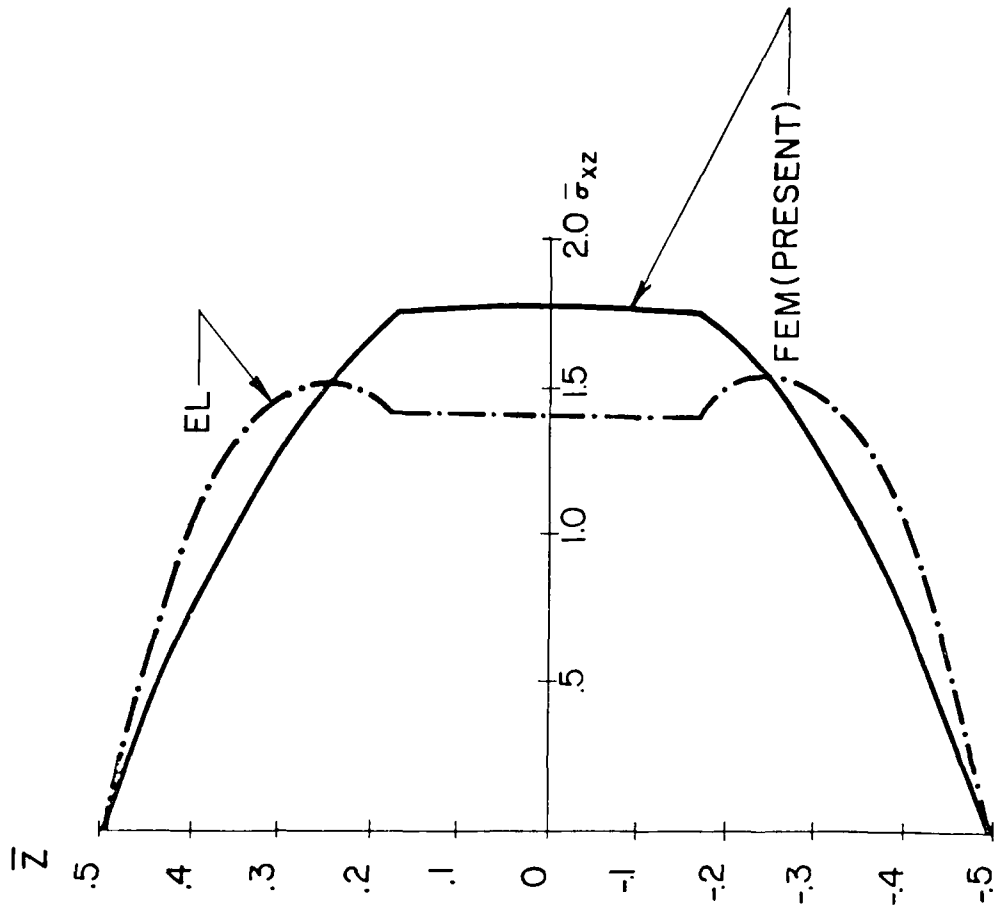


FIGURE 6: NORMALIZED TRANSVERSE SHEAR STRESS FOR CYLINDRICAL BENDING OF SYMMETRIC LAMINATE (S=4)

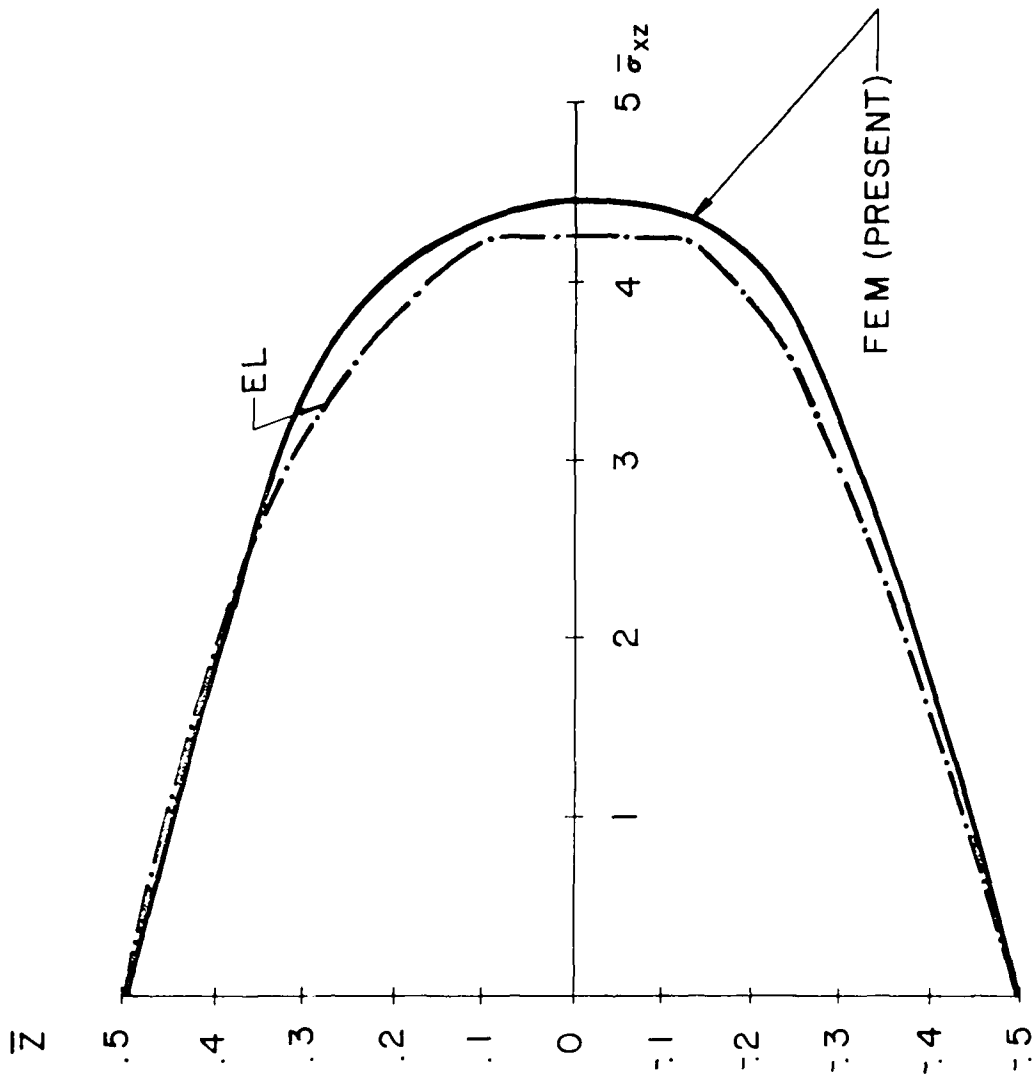


FIGURE 7: NORMALIZED TRANSVERSE SHEAR STRESS FOR CYLINDRICAL BENDING OF SYMMETRIC LAMINATE ($S=10$)

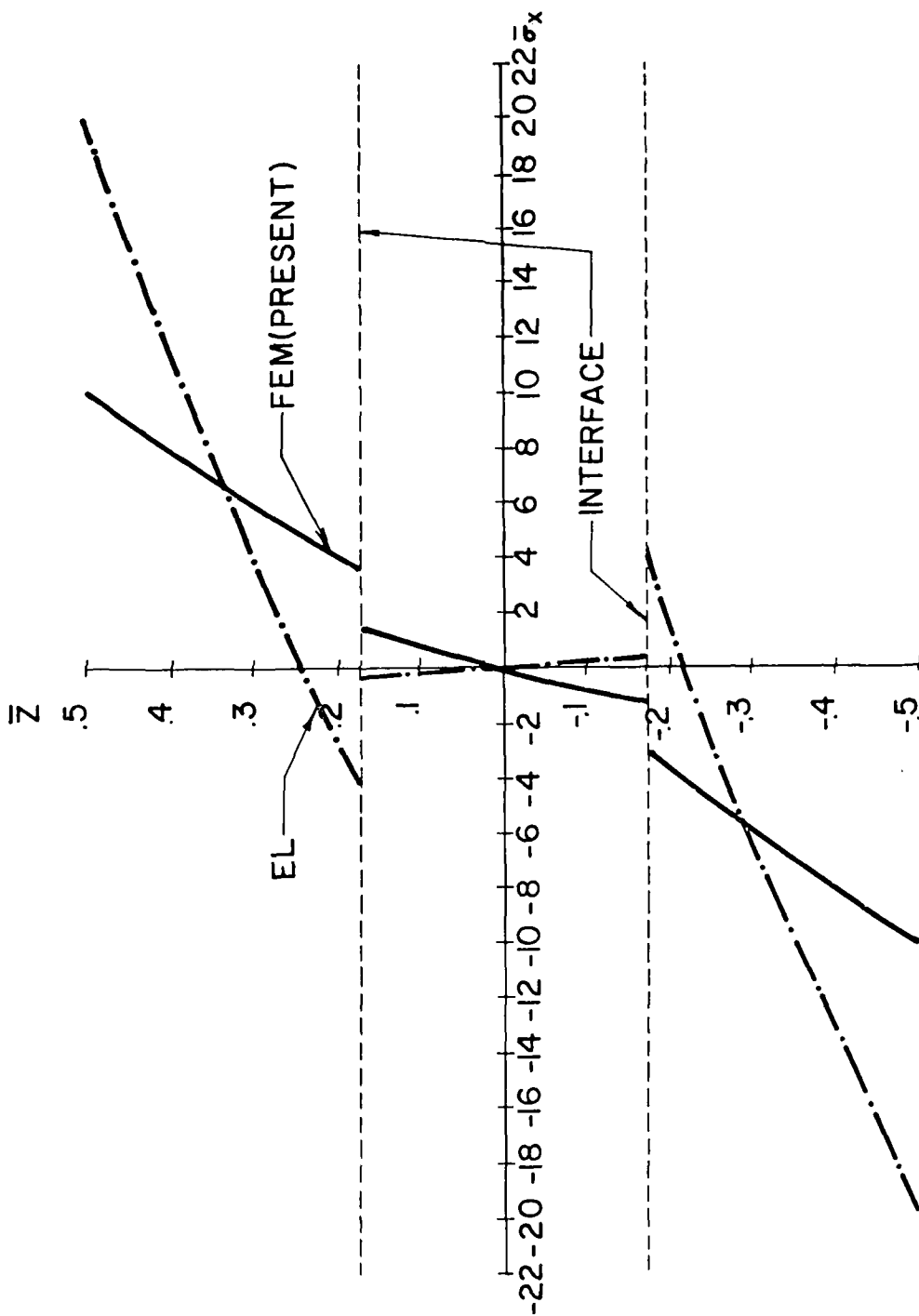


FIGURE 8: NORMALIZED IN-PLANE STRESS FOR CYLINDRICAL BENDING OF SYMMETRIC LAMINATE (S=4)

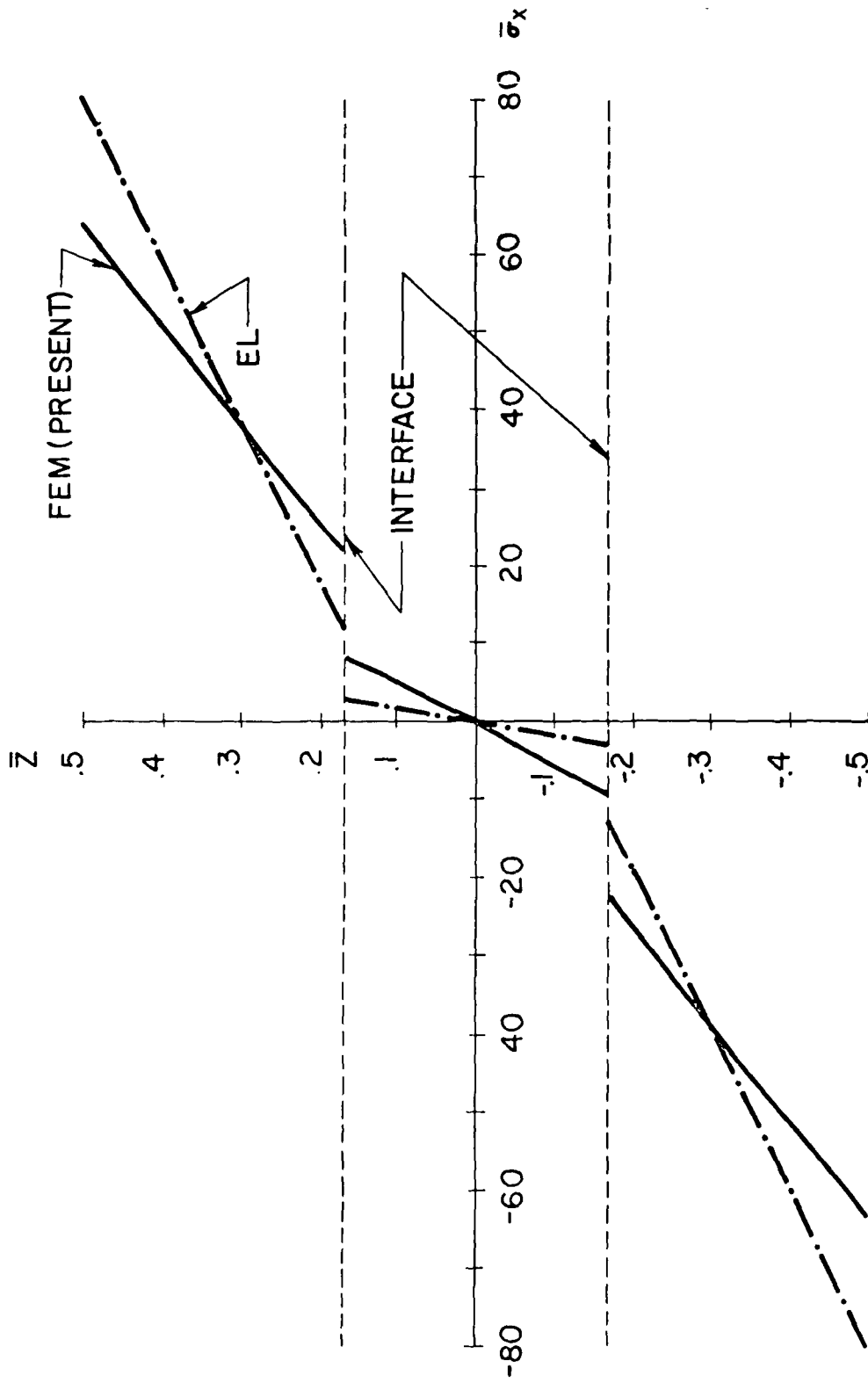


FIGURE 9: NORMALIZED IN-PLANE STRESS FOR CYLINDRICAL BENDING OF SYMMETRIC LAMINATE ($S=10$)

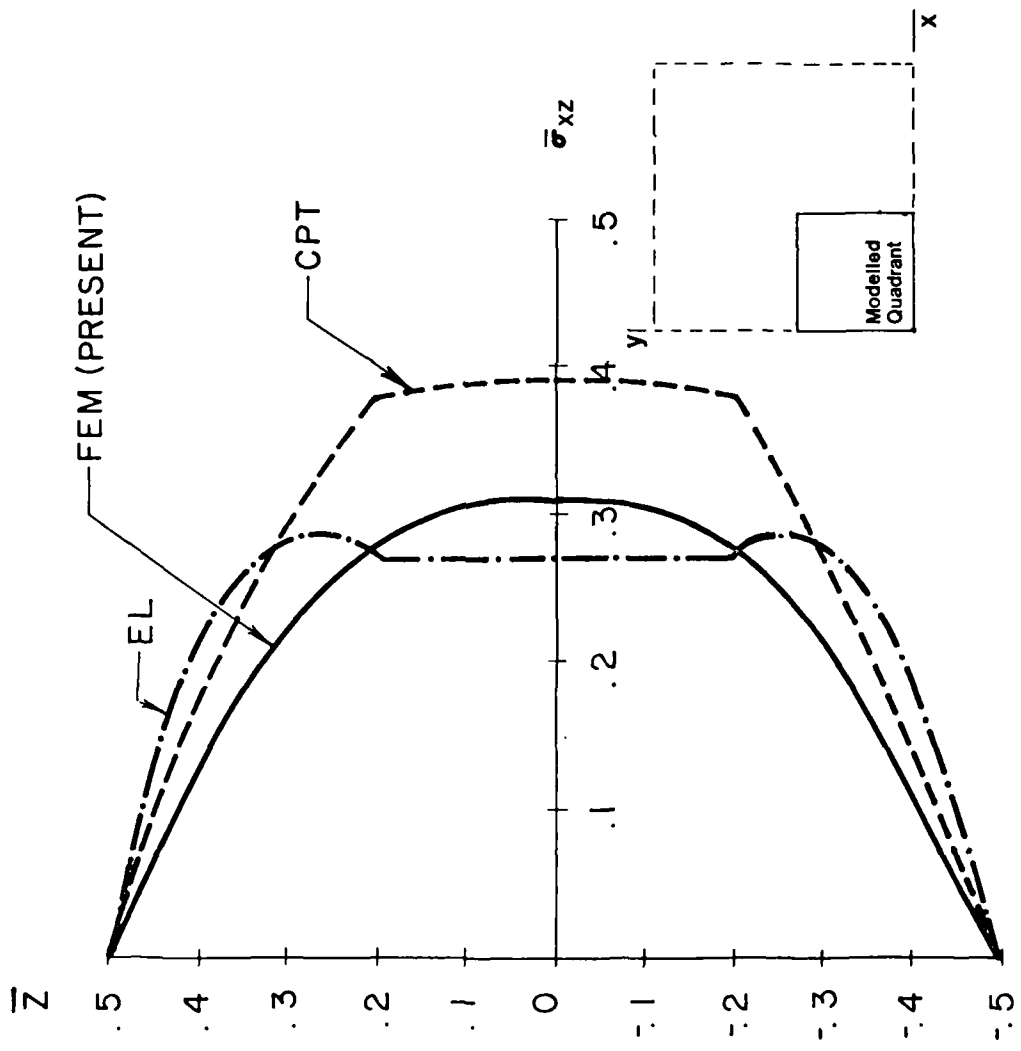


FIGURE 10: NORMALIZED TRANSVERSE SHEAR STRESS FOR SIMPLY SUPPORTED 0-90-0 SQUARE PLATE ($x=0, y=a/2, S=4$)

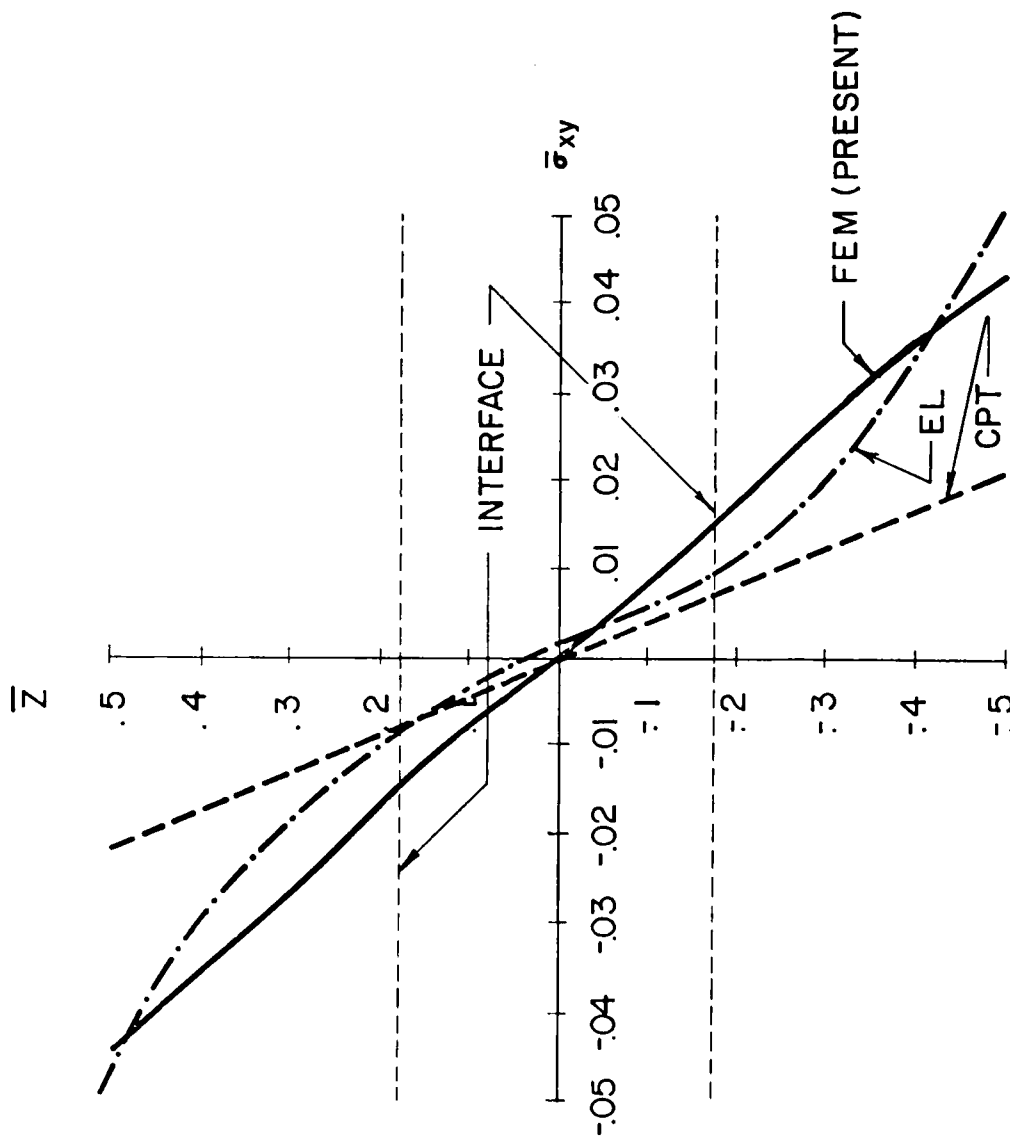


FIGURE 11: NORMALIZED IN-PLANE SHEAR STRESS FOR SIMPLY SUPPORTED 0-90-0 SQUARE PLATE ($x=0, y=0, S=4$)

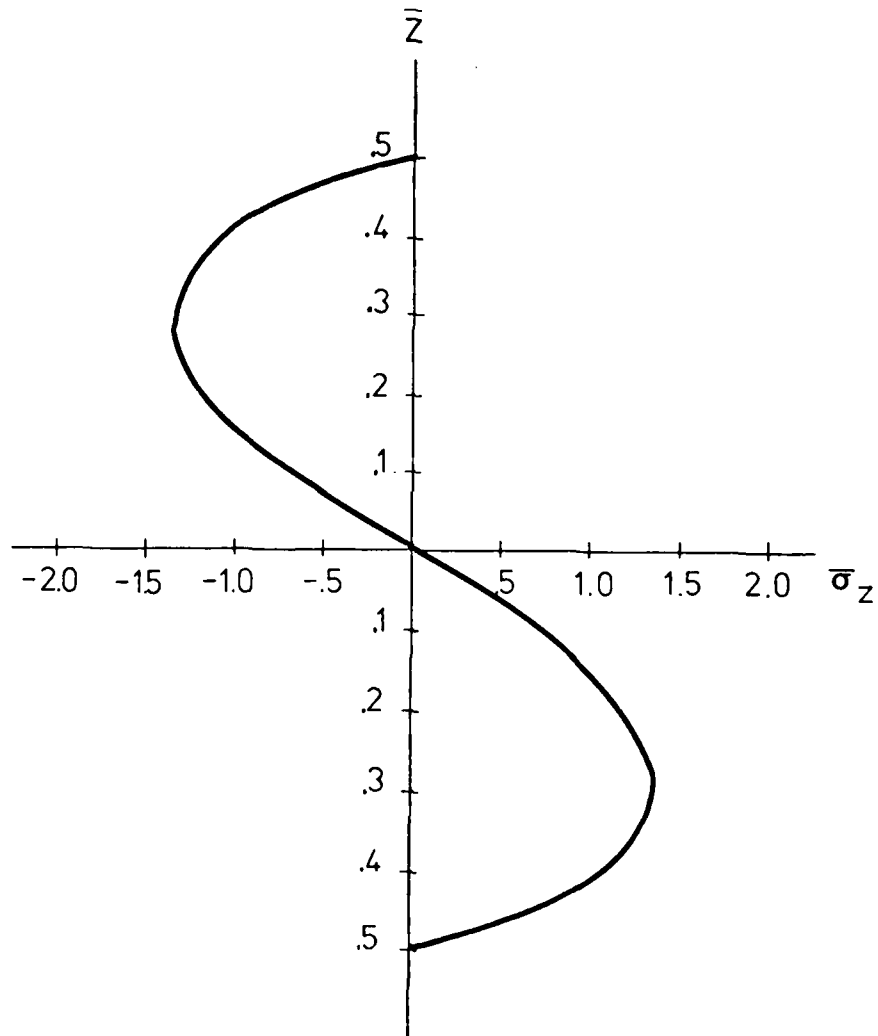


FIGURE 12: NORMALIZED SHORT-TRANSVERSE NORMAL STRESS FOR SIMPLY SUPPORTED 0-90-0 SQUARE PLATE ($x=a/2, y=0$)

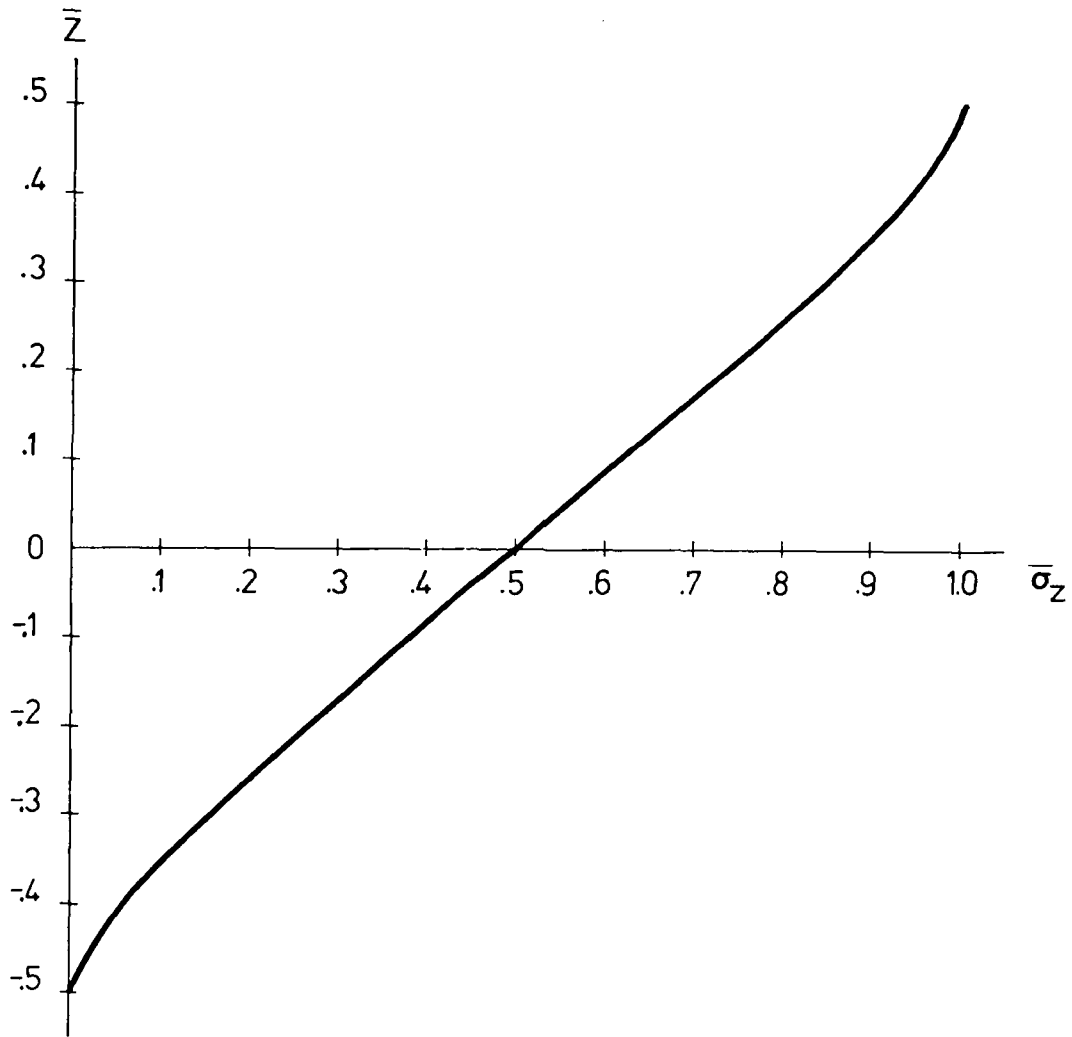


FIGURE 13: NORMALIZED SHORT-TRANSVERSE NORMAL STRESS FOR SIMPLY SUPPORTED 0-90-0 SQUARE PLATE ($x=a/2$, $y=a/2$)

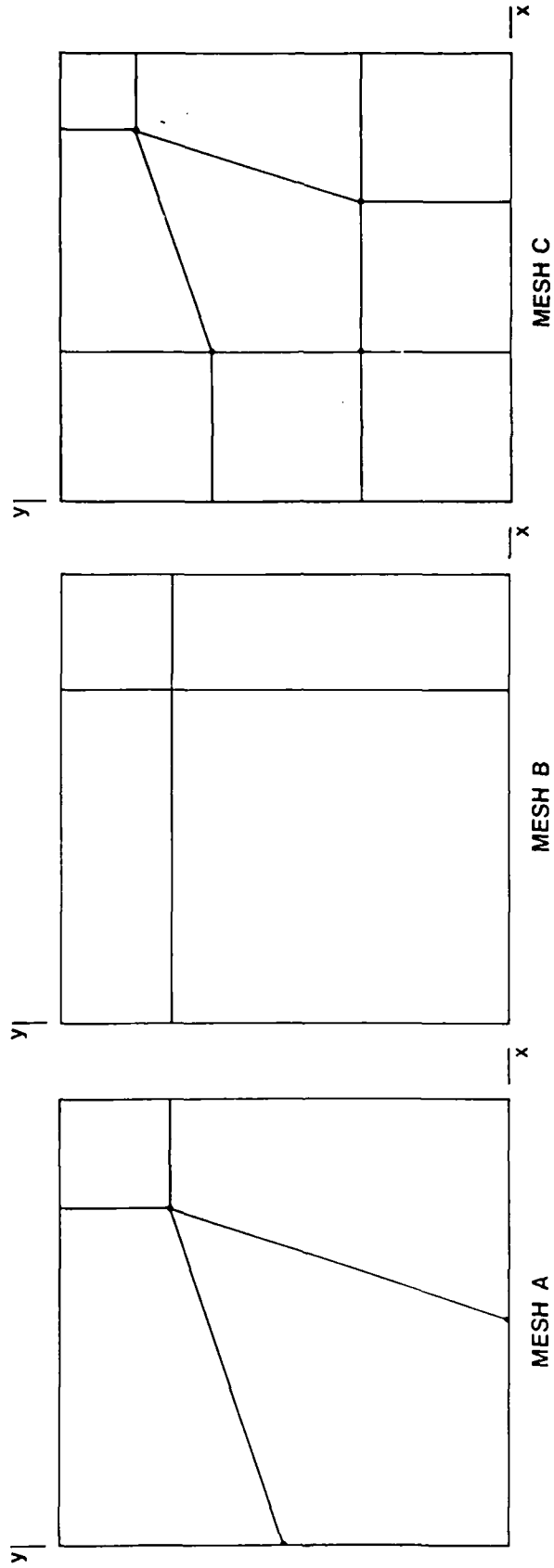


FIGURE 14: DISTORTED MESH GEOMETRIES

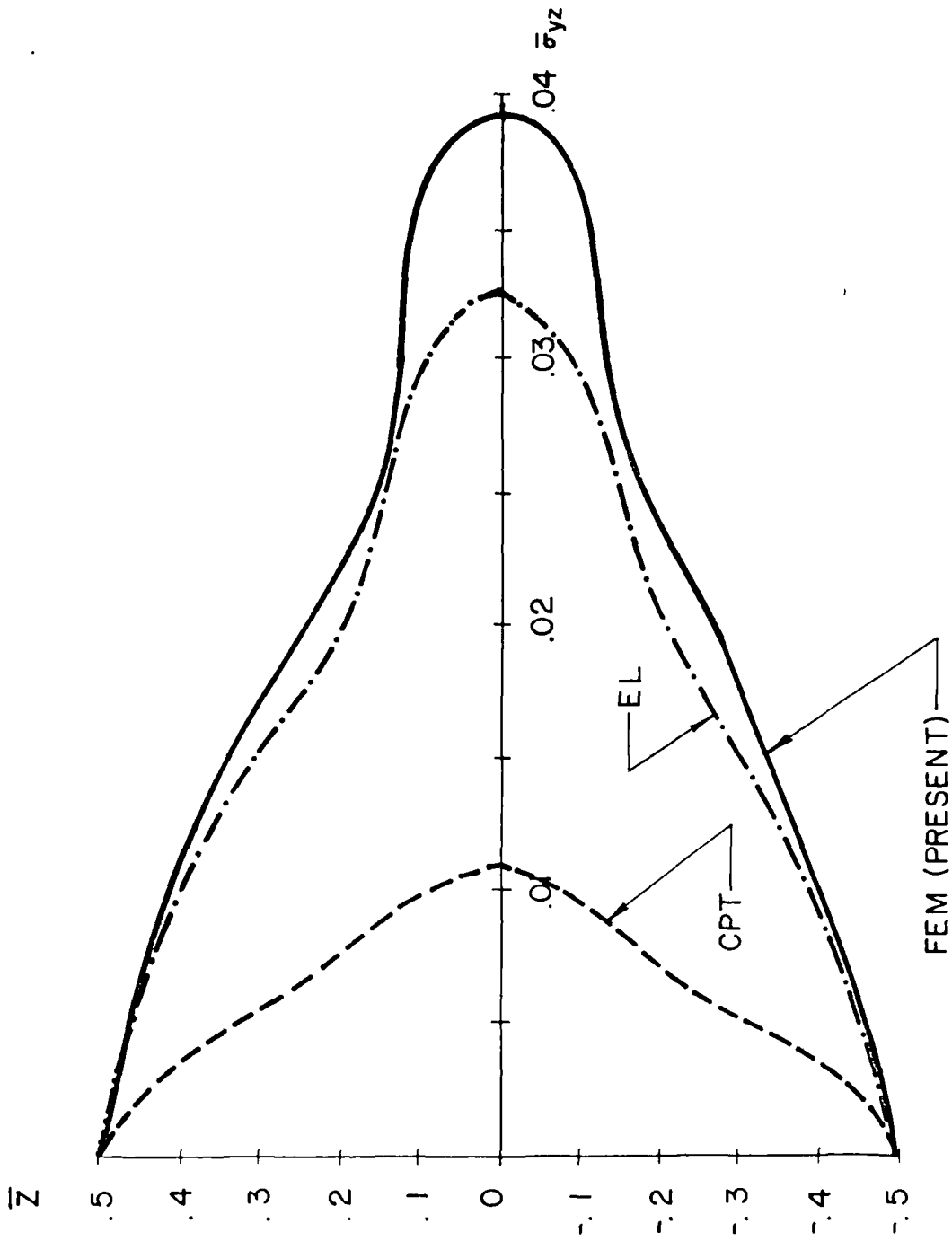


FIGURE 15: NORMALIZED TRANSVERSE SHEAR STRESS FOR SIMPLY SUPPORTED 0-90-0 RECTANGULAR PLATE ($x=a/2$, $y=0$, $S=4$)

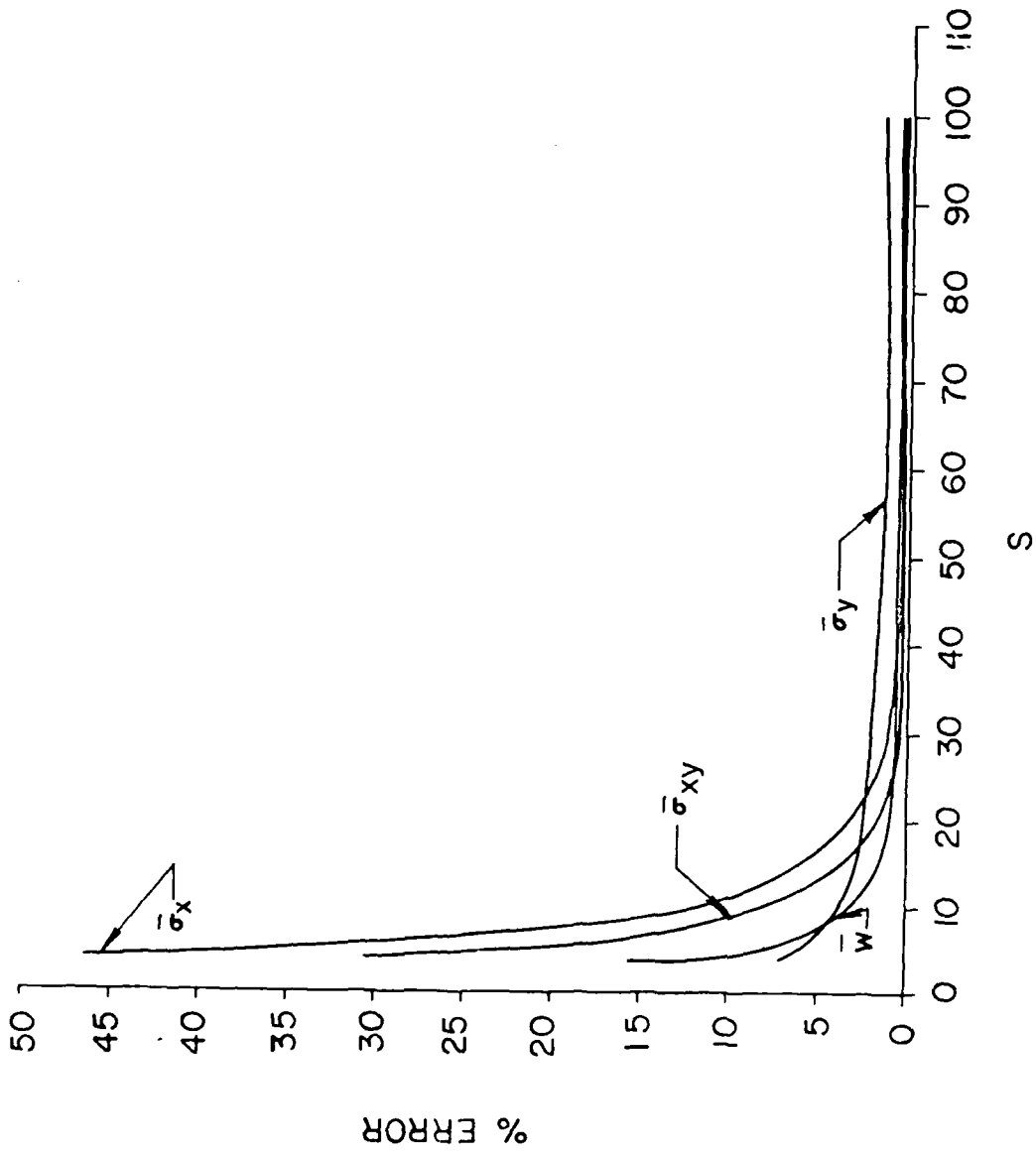


FIGURE 16: ERROR IN NORMALIZED DISPLACEMENT AND IN-PLANE STRESSES VS. ASPECT RATIO (REDUCED AND FULL INTEGRATION)

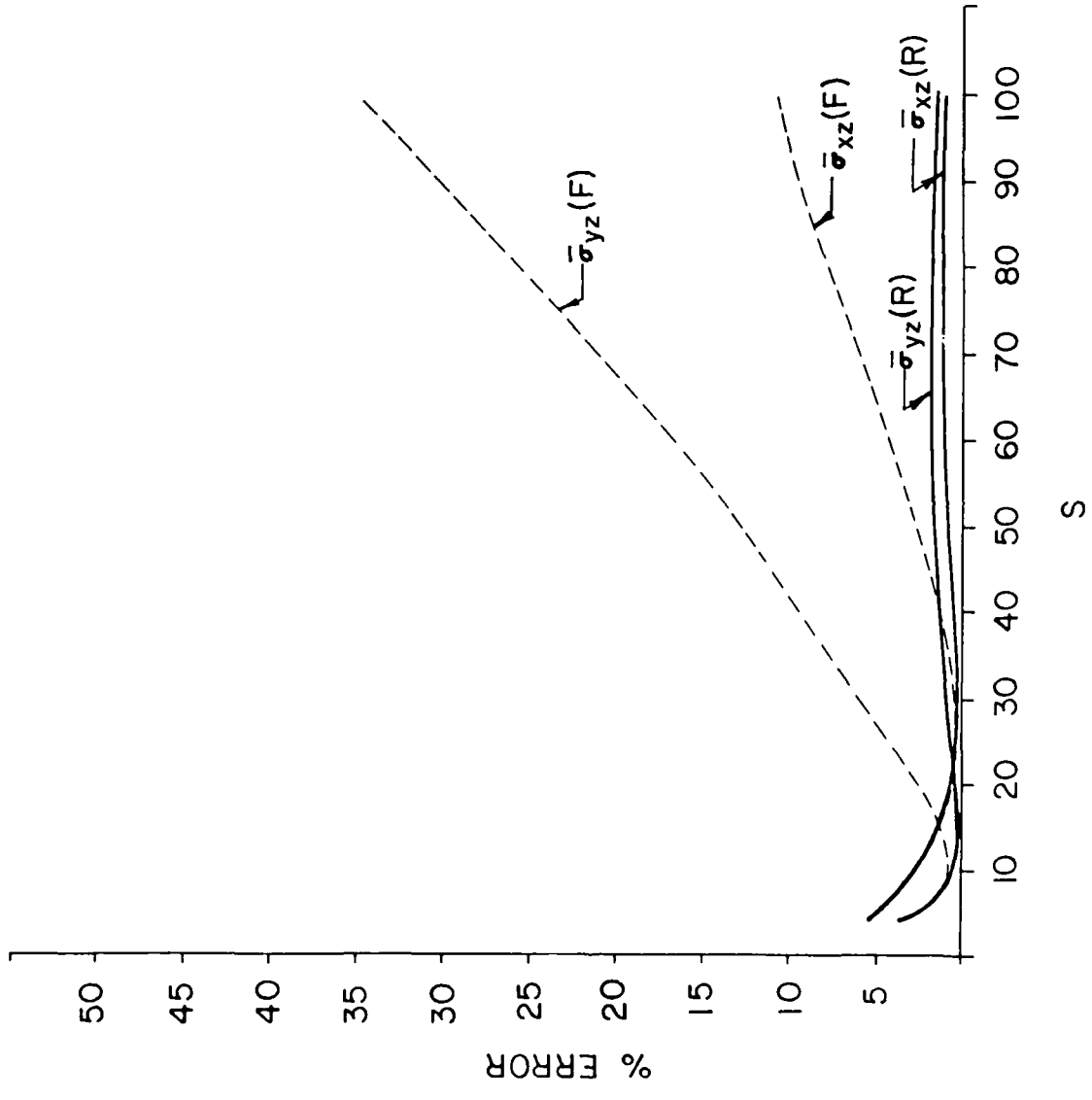


FIGURE 17: ERROR IN NORMALIZED TRANSVERSE SHEAR STRESSES VS. ASPECT RATIO (REDUCED AND FULL INTEGRATION)

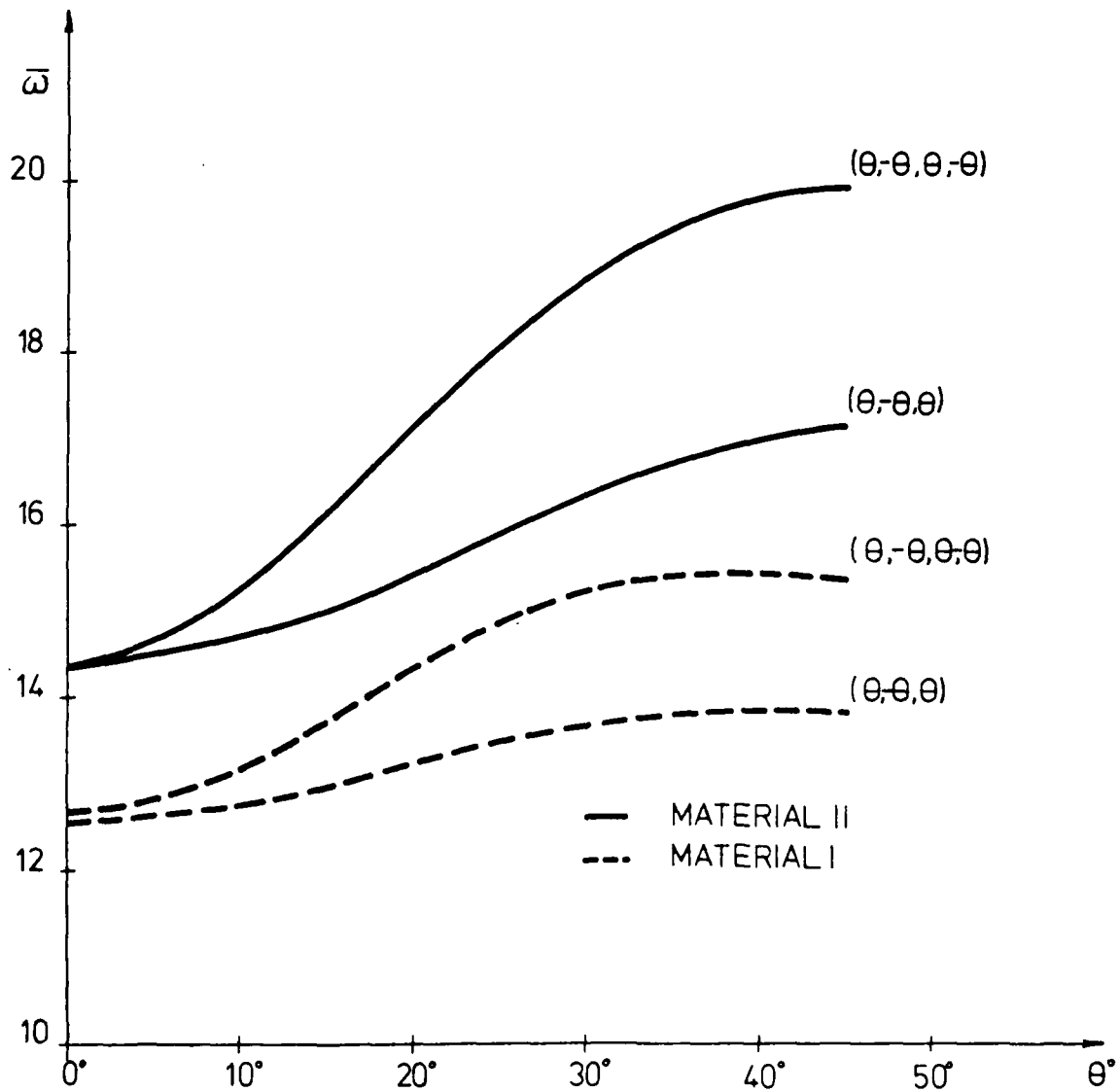


FIGURE 18: NON-DIMENSIONALIZED FUNDAMENTAL FREQUENCY VS. ANGLE OF PLY ORIENTATION FOR ANGLE-PLY, SIMPLY SUPPORTED, SQUARE PLATE OF PROBLEM 3

$$\bar{\omega} = \frac{a^2}{t} \sqrt{\frac{E_2}{E_1}}$$

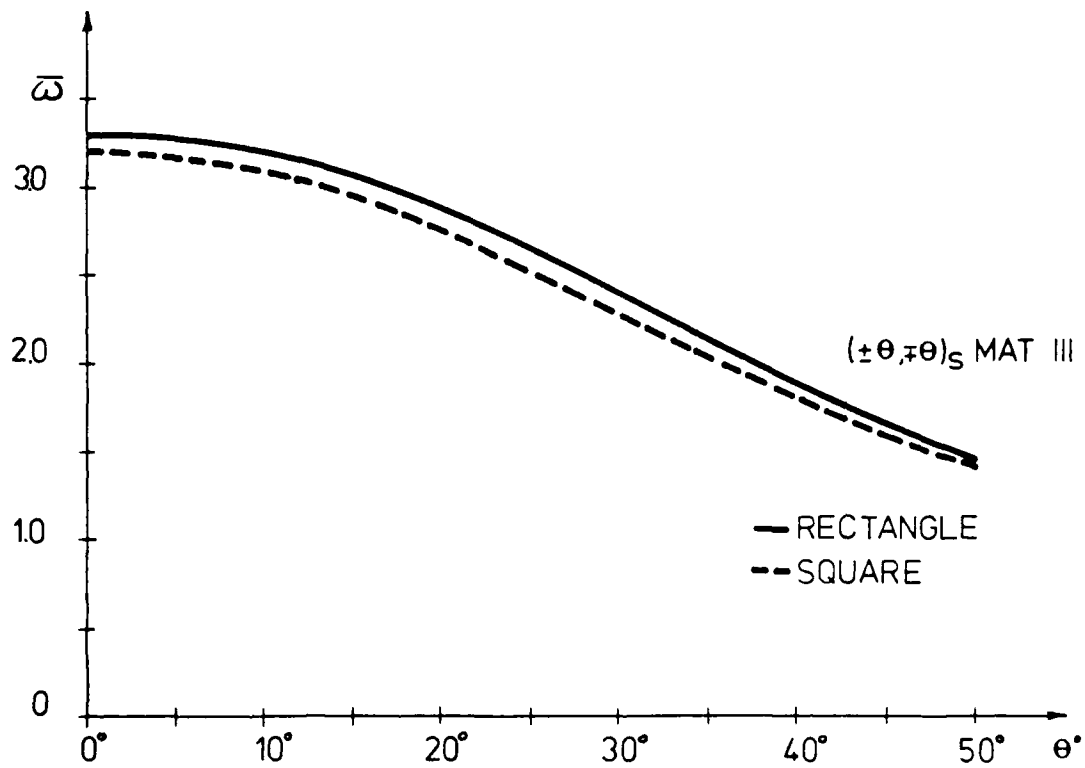


FIGURE 19: NON-DIMENSIONALIZED FUNDAMENTAL FREQUENCY VS. ANGLE OF PLY ORIENTATION FOR ANGLE-PLY, CANTILEVER PLATES OF PROBLEM 4

$$\omega = \frac{a^2}{l} \sqrt{E_2}$$

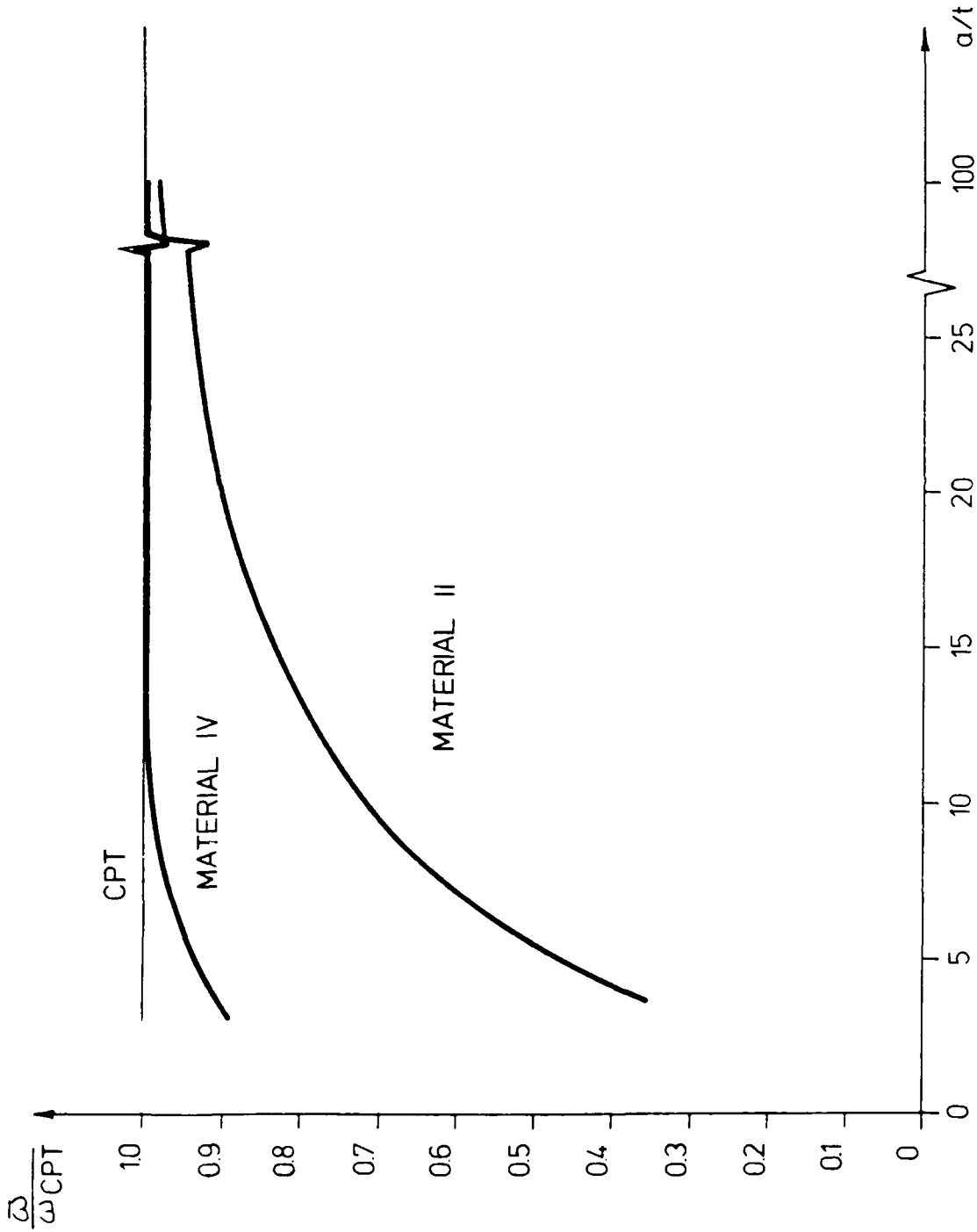


FIGURE 20: NORMALIZED FUNDAMENTAL FREQUENCY VS. ASPECT RATIO OF THE CYLINDRICAL BENDING PROBLEM.

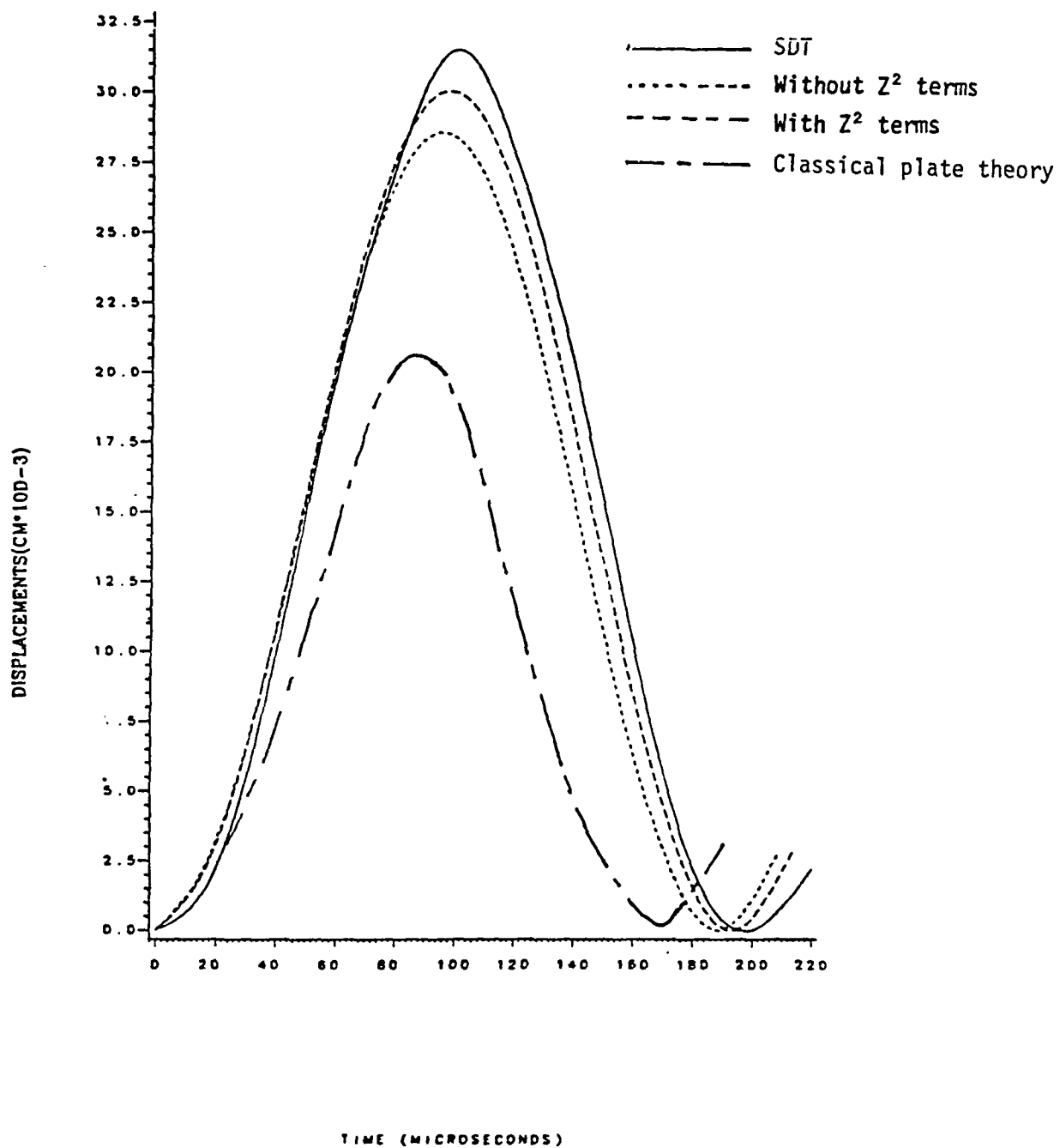


FIGURE 21: ONE-MODE DISPLACEMENT VS. TIME RESPONSE OF A COARSE-MESH (0/90) LAYUP SQUARE PLATE UNDER SUDDENLY-APPLIED SINUSOIDAL LOADING

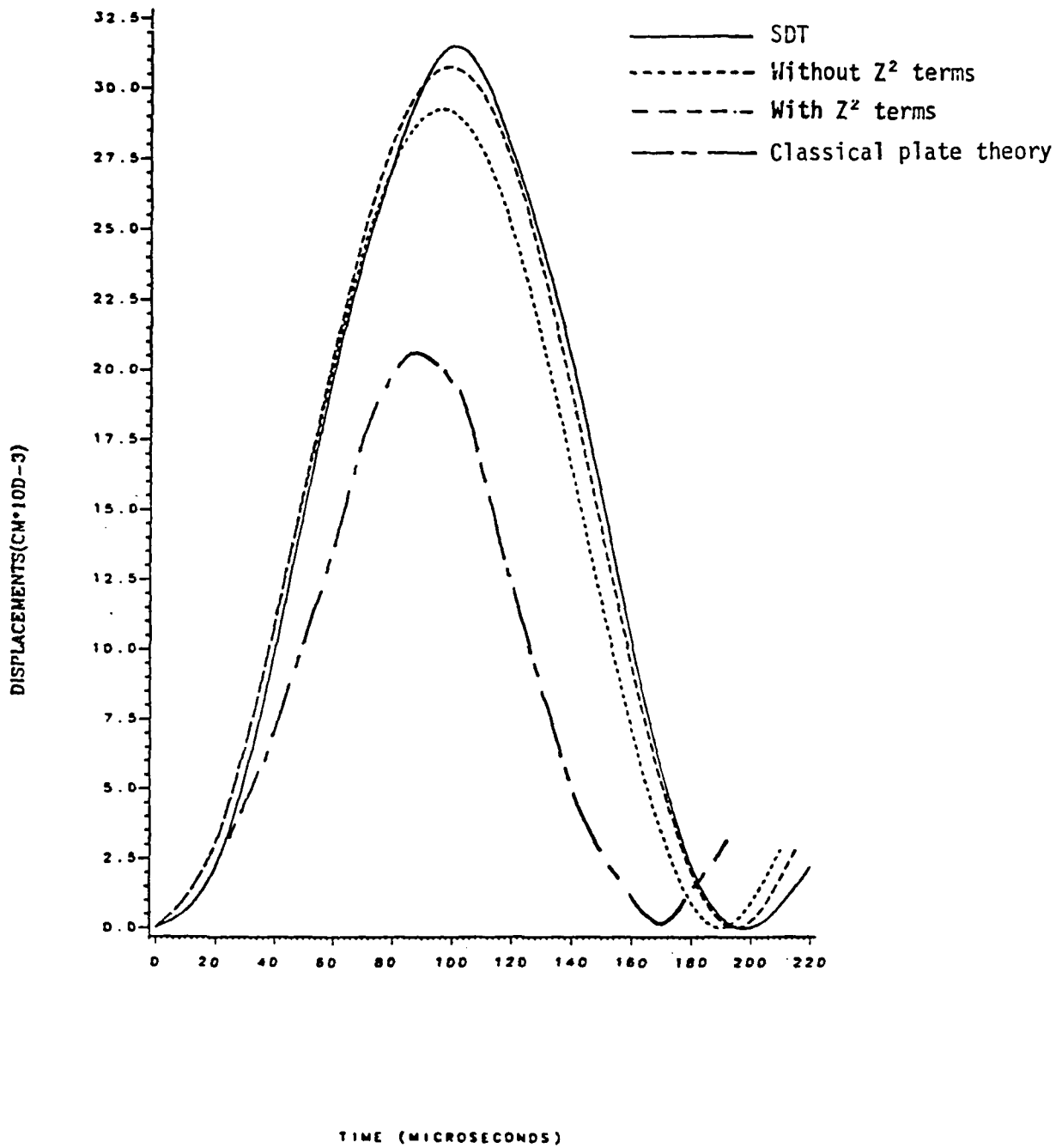


FIGURE 22: ONE-MODE DISPLACEMENT VS. TIME RESPONSE OF A FINE-MESH (0/90) LAYUP SQUARE PLATE UNDER SUDDENLY-APPLIED SINUSOIDAL LOADING

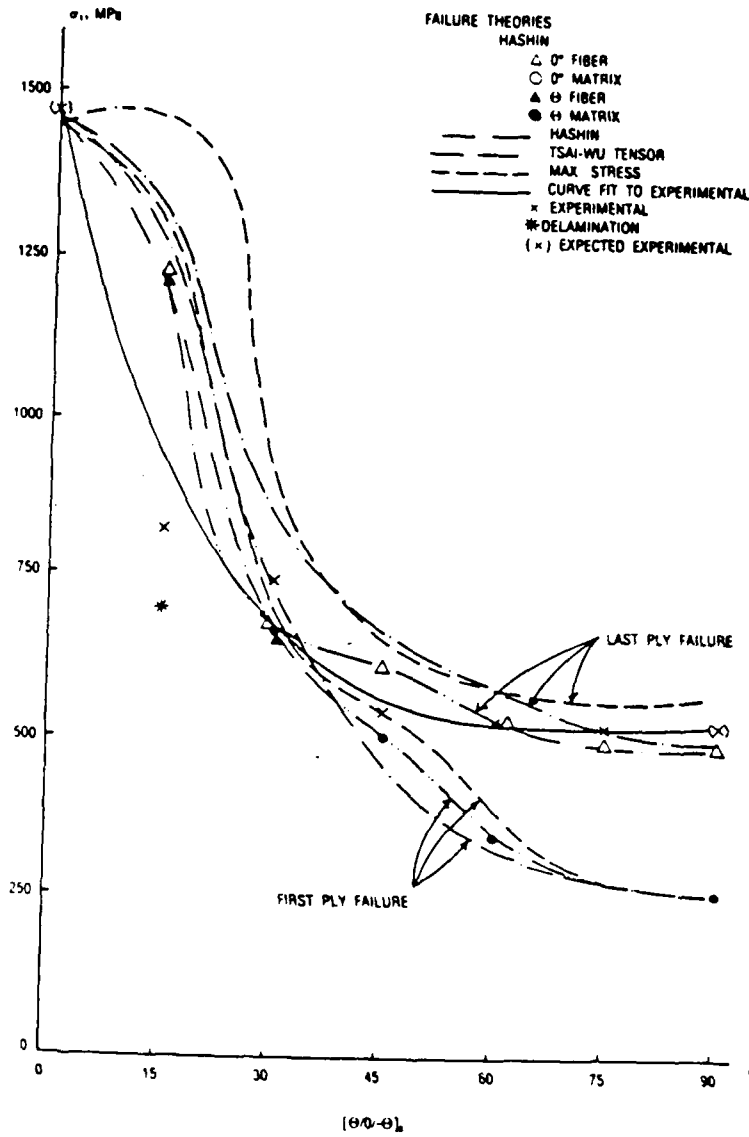


FIGURE 23: Failure Curves for $[\theta/0/-\theta]_s$ Tri-directional Laminates
Due to In-Plane Loading

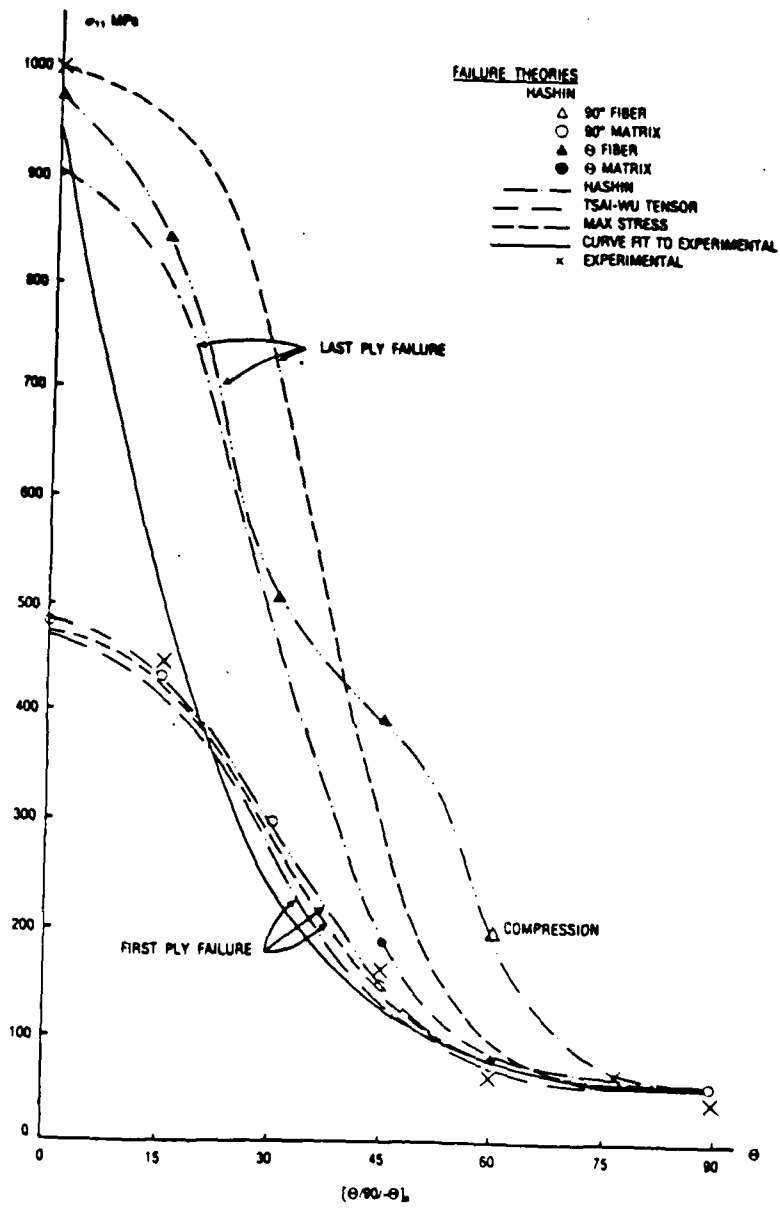


FIGURE 24: Failure Curves for $[\theta/90/-\theta]_s$ Tri-directional Laminates Due to In-Plane Loading

V. RELATED ACTIVITIES

Following is a list of abstracts and papers that have been submitted for presentation/publication as a result of the present research efforts.

Papers Accepted:

Journal of Sound and Vibration

"A Study of the Effects of Kinetic and Material Characteristics on the Fundamental Frequency Calculations of Composite Plates" O.O. Ochoa, J.J. Engblom, R.T. Tucker

Papers Submitted:

International Journal for Numerical Methods in Engineering

"Thru -the-Thickness Stress Predictions for Advanced Composite Material Configurations" J.J. Engblom and O.O. Ochoa

Conference Presentations:

SECTAM XII, Callaway Gardens, Georgia, May 9-11, 1983

"A Higher Order Displacement Formulation for Natural Vibration of Plates"

25th Structures, Structural Dynamics and Materials Conference, Palm Springs, California, May 14-16, 1984

"Through-the-Thickness Stress Predictions for Advanced Composite Material Configurations"

Symposium on Advances and Trends in Structures and Dynamics,

Washington, DC, October 22-25, 1984

"Inclusion of Damage Mechanisms in Finite Element Formulation of Composite Material Configurations"

Abstracts Submitted:

26th Structures, Structural Dynamics and Materials Conference,
Orlando, Florida, April 15-17, 1985

"Alternative Finite Element Approximations and Damage Prediction for Thin to Moderately Thick Fiber-Reinforced Composite Structures"

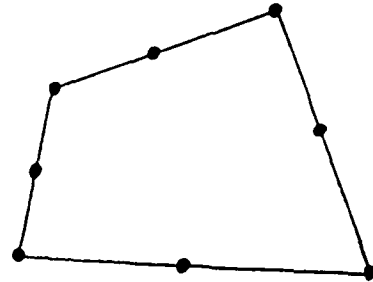
APPENDIX IA - HIGHER ORDER DISPLACEMENT MODELS

QHD40

NODAL DEGREES OF FREEDOM:

Corner Nodes - $\{u_0 \ v_0 \ w_0 \ \psi_x \ \psi_y \ \phi_x \ \phi_y\}^T$

Mid-side Nodes - $\{w_0 \ \psi_x \ \psi_y\}^T$



DISPLACEMENT FIELD:

$$u = u_0 + z\psi_x + z^2\phi_x$$

$$v = v_0 + z\psi_y + z^2\phi_y$$

$$w = w_0$$

where;

$$u_0, v_0, \phi_x, \phi_y : \{1 \ x \ y \ xy\}^T \{\alpha\}$$

$$w_0, \psi_x, \psi_y : \{1 \ x \ y \ x^2 \ xy \ y^2 \ x^3y \ xy^3\}^T \{\beta\}$$

STRESS FIELD:

i. From constitutive relations - $\sigma_{ij} = C_{ij}\epsilon_{ij}$ (orthotropic mat.)

$$\sigma_{xx} = f(z^2, x^2, y^2)$$

$$\sigma_{yy} = f(z^2, x^2, y^2)$$

$$\sigma_{xy} = f(z^2, x^2, y^2)$$

ii. From equilibrium considerations - $\sigma_{ij,j} = 0$

$$\sigma_{xz} = f(z^3, x, y)$$

$$\sigma_{yz} = f(z^3, x, y)$$

$$\sigma_{zz} = f(z^3)$$

QHD28

NODAL DEGREES OF FREEDOM:

$$\{u_0 \ v_0 \ w_0 \ \psi_x \ \psi_y \ \phi_x \ \phi_y\}^T$$

DISPLACEMENT FIELD:

$$u = u_0 + z\psi_x + z^2\phi_x$$

$$v = v_0 + z\psi_y + z^2\phi_y$$

$$w = w_0$$

where;

$$u_0, v_0, w_0, \psi_x, \psi_y, \phi_x, \phi_y, : \{1 \ x \ y \ xy\}^T \{\alpha\}$$

STRESS FIELD:

i. From constitutive relations - $\sigma_i = C_{ij}\epsilon_{ij}$ (orthotropic mat.)

$$\sigma_{xx} = f(z^2, x, y)$$

$$\sigma_{yy} = f(z^2, x, y)$$

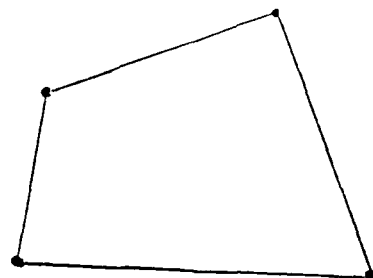
$$\sigma_{xy} = f(z^2, x, y)$$

ii. From constitutive considerations - $\sigma_{ij,j} = 0$

$$\sigma_{xz} = f(z^3)$$

$$\sigma_{yz} = f(z^3)$$

$$\sigma_{zz} = \text{constant}$$



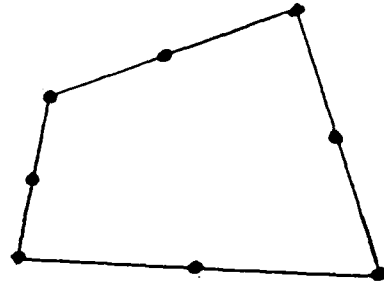
APPENDIX IB - MODIFIED KIRCHHOFF FORMULATION

QD32

NODAL DEGREES OF FREEDOM:

Corner Nodes $\{w_0 \ v_0 \ w \ \frac{\partial w}{\partial x} \ \frac{\partial w}{\partial y} \ \gamma_x \ \gamma_y\}^T$

Mid-Side Nodes $\{w \ \frac{\partial w}{\partial n}\}^T$



DISPLACEMENT FIELD:

$$w = f(x, y)$$

$$u = u_0 - z \left(\frac{\partial w}{\partial x} + \gamma_x \right)$$

$$v = v_0 - z \left(\frac{\partial w}{\partial y} + \gamma_y \right)$$

where;

$$u_0, v_0, \gamma_x, \gamma_y : \{1 \ x \ y \ xy\}^T \{\alpha\}$$

$$w = \{1 \ x \ y \ x^2 \ xy \ y^2 \ x^3 \ x^2y \ xy^2 \ y^3 \ x^4 \ x^3y \ xy^3 \ y^4 \ x^4y \ xy^4\}^T \{\beta\}$$

STRESS FIELD:

i. From constitutive relations - $\sigma_{ij} = C_{ij} \epsilon_{ij}$ (orthotropic mat.)

$$\sigma_{xx} = f(z, x^2, y^2)$$

$$\sigma_{yy} = f(z, x^2, y^2)$$

$$\sigma_{xy} = f(z, x^2, y^2)$$

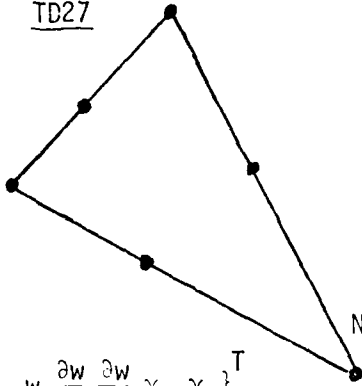
ii. From equilibrium considerations - $\sigma_{ij,j} = 0$

$$\sigma_{xz} = f(z^2, x^2, y^2)$$

$$\sigma_{yz} = f(z^2, x^2, y^2)$$

$$\sigma_{zz} = f(z^3, x, y)$$

TD27



$$\{u_0 \ v_0 \ w \ \frac{\partial w}{\partial x} \ \frac{\partial w}{\partial y} \ \gamma_x \ \gamma_y\}^T$$

$$\{w \ \frac{\partial w}{\partial n}\}^T$$

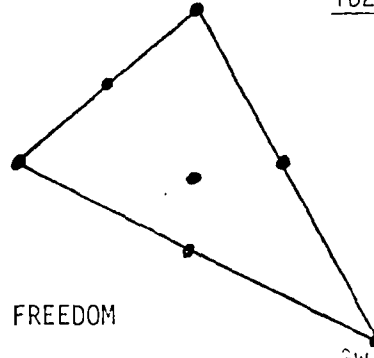
NODAL DEGREES OF FREEDOM

Corner Nodes

Mid-side Nodes

Center Node

TD27M



$$\{u_0 \ v_0 \ w \ \frac{\partial w}{\partial x} \ \frac{\partial w}{\partial y} \ \gamma_x \ \gamma_y\}^T$$

$$\{w\}^T$$

$$\{w \ \frac{\partial w}{\partial x} \ \frac{\partial w}{\partial y}\}^T$$

DISPLACEMENT FIELD

$$w = f(x, y)$$

$$u = u_0 - z \left(\frac{\partial w}{\partial x} + \gamma_x \right)$$

$$v = v_0 - z \left(\frac{\partial w}{\partial y} + \gamma_y \right)$$

where;

$$u_0, v_0, \gamma_x, \gamma_y : \{1 \ x \ y\}^T \{\beta\}$$

$$w : \{1 \ x \ y \ x^2 \ xy \ y^2 \ x^3 \ x^2y \ xy^2 \ y^3 \ x^4 \ x^3y \ x^2y^2 \ xy^3 \ y^4\}^T \{\beta\}$$

STRESS FIELD

i. From constitutive relations - $\sigma_{ij} = C_{ij} \epsilon_{ij}$ (orthotropic mat.)

$$\sigma_{xx} = f(z, x^2, y^2)$$

$$\sigma_{yy} = f(z, x^2, y^2)$$

$$\sigma_{xy} = f(z, x^2, y^2)$$

ii. From equilibrium considerations - $\sigma_{ij,j} = 0$

$$\sigma_{xx} = f(z^2, x, y)$$

$$\sigma_{yz} = f(z^2, x, y)$$

$$\sigma_{zz} = f(z^3)$$

APPENDIX II - HYBRID-STRESS FORMULATION

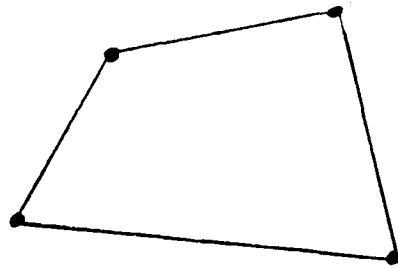
QHS32

DISPLACEMENT FIELD:

$$u = u_0 + z\psi_x + z^2\phi_x$$

$$v = v_0 + z\psi_y + z^2\phi_y$$

$$w = w_0 + z\phi_z$$



where;

$$u_0, v_0, \psi_x, \psi_y, \phi_z, \phi_x, \phi_y : \{1 \ x \ y \ xy\}^T \{\alpha\}$$

STRESS FIELD:

$$\sigma_x = (\beta_1 + \beta_2 x + \beta_3 y + \beta_4 xy) + z(\beta_5 + \beta_6 x + \beta_7 y + \beta_8 xy) + z^2(\beta_9 + \beta_{10} x + \beta_{11} y - \frac{3}{h^2}\beta_4 xy)$$

$$\sigma_y = (\beta_{12} + \beta_{13} x + \beta_{14} y - \beta_4 xy) + z(\beta_{15} + \beta_{16} x + \beta_{17} y + \beta_{18} xy) + z^2(\beta_{19} - \beta_{10} x - \beta_{11} y + \frac{3}{h^2}\beta_4 xy)$$

$$\sigma_{xy} = [\beta_{20} + (-\beta_{15} - \frac{h^2}{3}\beta_{21} + \frac{h^2}{3}\beta_{11})x + (-\beta_2 - \frac{h^2}{3}\beta_{10} - \frac{h^2}{3}\beta_{22})y + (-\beta_9 - \beta_{19})xy] + z[\beta_{23} + \beta_{24} x + \beta_{25} y + (-\frac{3}{h}\beta_9 - \frac{3}{h}\beta_{19})xy] + z^2[\beta_{26} + \beta_{21} x + \beta_{22} y + (\frac{3}{h^2}\beta_9 + \frac{3}{h^2}\beta_{19})xy]$$

$$\sigma_{xz} = (-h - z) [-\frac{h^2}{3}(\beta_{10} + \beta_{22}) + \beta_4 y + (-\beta_9 - \beta_{19})x] + \frac{1}{2}(h^2 - z^2)[\beta_6 + \beta_{25} + \beta_8 y - \frac{3}{h}(\beta_9 + \beta_{19})x]$$

$$+ \frac{1}{3}(-h^3 - z^3)[\beta_{10} - \frac{3}{h^2}\beta_4 y + \beta_{22} + \frac{3}{h^2}(\beta_9 + \beta_{19})x]$$

$$\sigma_{yz} = (-h - z) [-\frac{h^2}{3}\beta_{21} + \frac{h^2}{3}\beta_{11}] + (-\beta_9 - \beta_{19})y - \beta_4 x]$$

$$+ \frac{1}{2}(h^2 - z^2)[\beta_{24} - \frac{3}{h}(\beta_9 + \beta_{19})y + \beta_{17} + \beta_{18} x]$$

$$+ \frac{1}{3}(-h^3 - z^3)[\beta_{21} + \frac{3}{h^2}(\beta_9 + \beta_{19})y - \beta_{11} + \frac{3}{h^2}\beta_4 x]$$

$$\sigma_z = (\beta_9 + \beta_{19}) [-(h + z)^2 - \frac{(-2h^3 - 3h^2 z + z^3)}{h}] + (\frac{3h^4 + 4h^3 z + z^4}{2h})]$$

APPENDIX III - MASS MATRIX FORMULATION

The mass matrix for elements under development is easily arrived at by considering kinetic energy in the form

$$T = \frac{1}{2} \int_V \rho (\dot{u}^2 + \dot{v}^2 + \dot{w}^2) dV$$

where u , v and w represent displacements, ρ is the mass density and the dot superscript denotes velocity. Defining velocities in terms of element shape functions gives

$$T = \frac{1}{2} [\dot{\Delta}]^T \int_V \rho \{N_u\}[N_u] + \{N_v\}[N_v] + \{N_w\}[N_w] dV \{\dot{\Delta}\}$$

which is the classical form

$$T = \frac{1}{2} [\dot{\Delta}]^T [M] \{\dot{\Delta}\}$$

The element mass matrix $[M]$ is, therefore, specified as

$$[M] = \int_V \rho \{N_u\}\{N_u\} + \{N_v\}\{N_v\} + \{N_w\}\{N_w\} dV$$

Note that the shape functions $[N_i]$ involve distance from the mid-plane of the element to a layer denoted by Z and, therefore, the mass matrix definition provided not only represents mid-plane inertial effects but also rotatory inertia as well.

APPENDIX IV - LARGE DISPLACEMENT FORMULATION

Based on Green's Strain Tensor, the following procedure is utilized to obtain the large displacement and the geometric stiffness matrices.

Let N be shape functions relating displacements at any point in the element $\{\delta\}$ to nodal displacements $\{\Delta\}$ such that

$$\{\delta\} = [N]\{\Delta\}$$

Also let $\{N_{i,j}\}^T$ denote those shape functions associated with the i^{th} displacement field ($i - u, v, w$) and " j " denotes the differentiation with respect to the j^{th} coordinate, i.e., $\frac{\partial}{\partial x_j}$ where $x_1 = x$, $x_2 = y$ and $x_3 = z$. Then, the strain ϵ_{xx} given by

$$\epsilon_{xx} = \frac{\partial u}{\partial x} + \frac{1}{2} \left[\left(\frac{\partial u}{\partial x} \right)^2 + \left(\frac{\partial v}{\partial x} \right)^2 + \left(\frac{\partial w}{\partial x} \right)^2 \right]$$

can be written as

$$\epsilon_{xx} = \{N_{u,x}\}^T \{\Delta\} + \frac{1}{2} \{\Delta\}^T \left[\{N_{u,x}\}^T \{N_{u,x}\} + \{N_{v,x}\}^T \{N_{v,x}\} + \{N_{w,x}\}^T \{N_{w,x}\} \right] \{\Delta\}$$

Similarly, the shear strain ϵ_{xy} can be represented by

$$\begin{aligned} \epsilon_{xy} = & \left\{ \{N_{u,y}\}^T + \{N_{v,x}\}^T \right\} \{\Delta\}^T + \{\Delta\}^T \left\{ \{N_{u,x}\}^T \{N_{u,y}\} + \{N_{v,x}\}^T \{N_{v,y}\} \right. \\ & \left. + \{N_{w,x}\}^T \{N_{w,y}\} \right\} \{\Delta\} \end{aligned}$$

The strain field in indicial notation is expressed by

$$\{\epsilon_{ij}\} = \frac{1}{2} \left\{ \left[\{N_{i,j}\}^T + \{N_{j,i}\}^T \right] \{\Delta\} + \{\Delta\}^T \left[\{N_{k,i}\}^T \{N_{k,j}\} \right] \{\Delta\} \right\}$$

Then the incremental representation becomes

$$\{\delta \varepsilon_{ij}\} = \frac{1}{2} \left[\{N_{i,j}\}^T + \{N_{j,i}\}^T \right] \{\delta \Delta\} + \{\delta \Delta\}^T \left[\{N_{k,i}\}^T \{N_{k,j}\} \right] \{\Delta\} + \{\Delta\}^T \left[\{N_{k,i}\}^T \{N_{k,j}\} \right] \{\delta \Delta\}$$

But the second term can be expressed as

$$\{\Delta\}^T \left[\{N_{k,j}\}^T \{N_{k,i}\} \right] \{\delta \Delta\}$$

Thus combining terms

$$\{\delta \varepsilon_{ij}\} = \frac{1}{2} \left[\left[\{N_{i,j}\}^T + \{N_{j,i}\}^T \right] \{\delta \Delta\} + \{\Delta\}^T \left[\{N_{k,i}\}^T \{N_{k,j}\} + \{N_{k,j}\}^T \{N_{k,i}\} \right] \{\delta \Delta\} \right]$$

Let

$$[B_0] = \frac{1}{2} \left[\{N_{i,j}\}^T + \{N_{j,i}\}^T \right]$$

$$[B_L] = \frac{1}{2} \{\Delta\}^T \left[\{N_{k,i}\}^T \{N_{k,j}\} + \{N_{k,j}\}^T \{N_{k,i}\} \right] =$$

$$\begin{bmatrix} \{\Delta\}^T [M_{xx}] \\ \{\Delta\}^T [M_{yy}] \\ \{\Delta\}^T [M_{xy}] \\ \{\Delta\}^T [M_{zz}] \\ \{\Delta\}^T [M_{xz}] \\ \{\Delta\}^T [M_{yz}] \end{bmatrix}$$

Then

$$\{\delta \Delta_{ij}\} = [B_0] \{\delta \Delta\} + [B_L] \{\delta \Delta\}$$

where $[B_0]$ is the linear component and $[B_L]$ is the large displacement component. Having the definitions for $[B_0]$ and $[B_L]$, the small and large displacement matrices $[K_0]$ and $[K_L]$ are represented as

$$[K_0] = \int_V [B_0]^T [D] [B_0] dV$$

$$[K_L] = \int_V \left\{ [B_L]^T [D] [B_0] + [B_L]^T [D] [B_L] + [B_0]^T [D] [B_L] \right\} dV$$

The geometric stiffness matrix is also derived from $[B_L]$ and it has the following form

$$[KG] = \int_V \left(\sigma_{xx}[M_{xx}] + \sigma_{yy}[M_{yy}] + \sigma_{zz}[M_{zz}] + \sigma_{xy}[M_{xy}] + \sigma_{xz}[M_{xz}] + \sigma_{yz}[M_{yz}] \right) dV$$

Where the σ 's are the stress components and again integration is on a layer by layer basis.

END

FILMED

3-86

DTIC